U.PORTO

FEUP **FACULDADE DE ENGENHARIA**
UNIVERSIDADE DO PORTO

Airborne Wind Energy Systems: Modelling, Simulation and Trajectory Control

Gonçalo Barros da Silva

Mestrado Integrado em Engenharia Eletrotécnica e de Computadores

Supervisor: Fernando Arménio da Costa Castro e Fontes

Co-Supervisor: Luís Tiago de Freixo Ramos Paiva

July 30, 2018

Resumo

Atualmente a energia eólica é essencialmente extraída on-shore através de turbinas eólicas com algumas dezenas de metros. No entanto, é off-shore e a elevadas altitudes que o vento é mais forte e, sobretudo, mais consistente. Neste contexto, soluções inovadoras no âmbito dos AWES têm vindo a ser apresentadas.

Com esta dissertação pretende-se estudar um destes sistemas, que envolve um kite ligado a um gerador através de um cabo. À medida que o kite se eleva por força do vento, o cabo é desenrolado, fazendo acionar o gerador, produzindo assim energia. Posteriormente, o cabo é recolhido e, de seguida, o processo repete-se. O sucesso destes sistemas é suportado pelo facto de que a força de *lift* do kite é proporcional ao quadrado da velocidade aparente do vento. O objectivo principal desta dissertação é desenvolver um algoritmo de seguimento de trajetória que permita ao kite seguir um caminho pré-definido durante a fase de produção. A trajetória deve ser definida de forma a que o kite se mova maioritariamente numa direção perpendicular à velocidade do vento, maximizando assim a produção de energia.

Neste contexto, o modelo dinâmico 3D do Kite é descrito. De seguida, são realizadas simulações com versões 2D simplificadas do modelo, com o objetivo de o validar. Posteriormente, é desenvolvido um controlador de trajetória para seguir um caminho desejado, que inclui um modo inovador de rajadas de vento. A estratégia apresentada permite-nos lidar com fortes velocidades de vento, impedindo que o sistema seja danificado, sem ter que retrair completamente o kite. Por fim, desenvolvemos outro algoritmo de seguimento de trajetória baseado numa *Nonlinear Guidance Logic* e demonstramos estabilidade com base numa análise de Lyapunov.

Abstract

Currently wind power is essentially extracted on-shore through wind turbines with a few tens of meters. However, it is off-shore and at high altitudes that the wind is stronger and, above all, more consistent. In this context, innovative solutions within AWES have been presented.

With this dissertation we intend to study one of these systems, which involves a kite connected to a generator through a tether. As the kite rises by the wind, the cable is unrolled, causing the generator to start and thus producing energy. Subsequently, the cable is collected and then the process is repeated. The success of such systems is supported by the fact that the aerodynamic lift of the kite is proportional to the square of the apparent wind velocity. This dissertation main focus is to develop a path-following algorithm that allows the kite to follow a pre-defined path. The path should be one where the kite moves mainly in a perpendicular direction to the wind velocity during the production phase, maximizing energy production.

In this context, we describe the 3D dynamic model for the Kite Power System. Then, we do simulations with simplified 2D versions of the model, in order to validate it. Afterwards, a trajectory controller to follow a desired path is developed, which includes an innovative wind gust mode. Such strategy allow us to handle strong wind velocities, preventing the system to crash, without having to completely retract the kite. Finally, we develop another path follow algorithm based on a nonlinear guidance logic and show stability properties based on Lyapunov stability analysis.

Acknowledgments

I would like to thank my supervisors Fernando Fontes and Luís Tiago Paiva for the tremendous help they gave me during this dissertation, not only in teaching but also for all the motivation and strength they gave me to continue the work, even in the most difficult moments. Always available to answer any question, I thank them for all the patience they had, never giving up on me and helping me finish this work. Also, I want to thank my work colleague Manuel Fernandes for all the help and incentives.

I must as well thank my family, my mother, father and brother, for all the support they gave me. In the past few months I had many sleepless nights, and they were always there for me in those moments of despair, trying to calm me down and giving me the confidence to get up everyday and do the best work I could. I thank them for giving me the possibility of achieving this important goal in my life.

Also, I want to thank to all my friends for all the great moments we spent together that made me the person I am today. A special thanks to those who, in the last couple of months, had the patience to hear me complaining every day and still tried to cheer me up and motivate me to continue the work.

Gonçalo Silva

"Sexta Regra de Ouro: Sem Medo!"

Manuel C. R. M. Fernandes

Contents

List of Figures

List of Tables

List of Acronyms

AWE   Airborne Wind Energy
AWEC   Airborne Wind Energy Conference
AWES   Airborne Wind Energy System
FG   Fly-Gen
FG-AWES   Fly-Gen Airborne Wind Energy System
GG   Ground-Gen
GG-AWES   Ground-Gen Airborne Wind Energy System
HWE   High Wind Energy
KPS   Kite Power System

Nomenclature

A	wing reference area of kite $\left[\mathrm{m}^2\right]$
$\mathcal{R}$	wing aspect ratio
a_t	tether reel–out acceleration $\left[\mathrm{m\,s}^{-2}\right]$
c_D	aerodynamic drag coefficient
c_L	aerodynamic lift coefficient
E	energy produced [Ws]
$\vec{\mathrm{F}}^\mathrm{aer}$	aerodynamic force [N]
$\vec{\mathrm{F}}^\mathrm{drag}$	drag force [N]
$\vec{\mathrm{F}}^\mathrm{cent}$	centrifugal force [N]
$\vec{\mathrm{F}}^\mathrm{cor}$	Coriolis force [N]
$\vec{\mathrm{F}}^\mathrm{lift}$	aerodynamic lift force [N]
$\vec{\mathrm{F}}^\mathrm{inert}$	inertial forces [N]
$\vec{\mathrm{F}}^\mathrm{th}$	tether force [N]
g	gravitational acceleration $\left[\mathrm{m\,s}^{-2}\right]$
m	mass [kg]
P	power produced [W]
$\mathbf{p}$	kite position [m]
R_GL	rotation matrix from G to L
R_LG	rotation matrix from L to G
r	tether length [m]
ρ	fluid density $\left[\mathrm{kg\,m}^{-3}\right]$
T	tether tension [N]
$\mathbf{v}_a$	apparent fluid velocity $\left[\mathrm{m\,s}^{-1}\right]$
$\mathbf{v}_w$	fluid velocity $\left[\mathrm{m\,s}^{-1}\right]$
v_t	tether reel–out velocity $\left[\mathrm{m\,s}^{-1}\right]$
$\mathbf{u}$	control vector
$\mathbf{x}$	state vector
α	angle of attack [rad]
ϕ	azimuthal angle [rad]
β	elevation angle [rad]
ψ	roll angle [rad]
γ	reference tracking angle [rad]
τ	local tangent plane

Preface

This dissertation is part of the UPWind project, which studies Airborne Wind Energy Systems. The idea of generating power with tethered wings flying at high speed in a cross wind direction has been first proposed by Miles Loyd in 1980 [1]. Since then, a great variety of proposals has been reported. There are open research questions, involving challenging optimization and control issues. This project aims to contribute to answer some of these questions, namely

- Identification, Modelling and Estimation of AWES

- Optimization and Control of AWES

- Multiple Kite Systems

In this dissertation we focus on the trajectory control of the kite, designing controllers that allow the kite to follow a desired pre-defined path. Also, in Chapter 5 we develop an innovative wind gust mode to handle strong wind velocities in a safe way, preventing strong tether tensions that could be above the tether physical limit. The results obtained in this chapter were submitted to a conference and are accepted to publication in its proceedings [2].

Chapter 1

Introduction

1.1 Context

The demand for electrical energy is rising fast, as it is crucial to satisfy modern humans needs. Currently, the majority of electrical energy generated comes from non-renewable sources, such as fossil and nuclear fuels. However, it is unavoidable to reduce the consumption of such sources due to environmental sustainability.

In this context, there has been an increasing encouragement to the use of renewable energies which has lead to a fast growth and development of renewable energy systems over the last few years. One example of that is Portugal, as in March 2018, the total renewable energy production in the country exceeded the electricity consumed during that month [3]. Among the renewable energy sources, wind is an important large scale alternative. By the end of 2017, the overall capacity of all wind turbines installed worldwide reached 539MW, with Denmark setting a new world record with 43% of its power coming from wind [4]. While wind turbines are by far the most common and developed wind energy systems, their high cost and size limitations has lead to the development of some innovative alternatives.

One of the rising technologies is in the area of Airborne Wind Energy (AWE), more specifically Kite Power Systems (KPS) [5, 6]. These systems use a kite, with flexible or rigid wings, that is connected to a generator in the ground, through a cable (usually called tether). As the kite is elevated by the wind, the cable is unrolled, which causes the generator to start. When it reaches its maximum length, the cable is retracted and then the whole process is repeated.

It is known that, in these systems, the maximum power to be extracted from the wind is obtained when the kite moves in a direction perpendicular to the direction of the wind, which requires this trajectory to be periodic, for example, forming a circular or eight-shaped figure. Thus, it is necessary to design a controller to follow those paths.

1.2   Motivation

Currently, wind power is essentially extracted on-shore at low heights by conventional wind turbines. However, it is known that wind is much more powerful and consistent off-shore and at high altitudes.
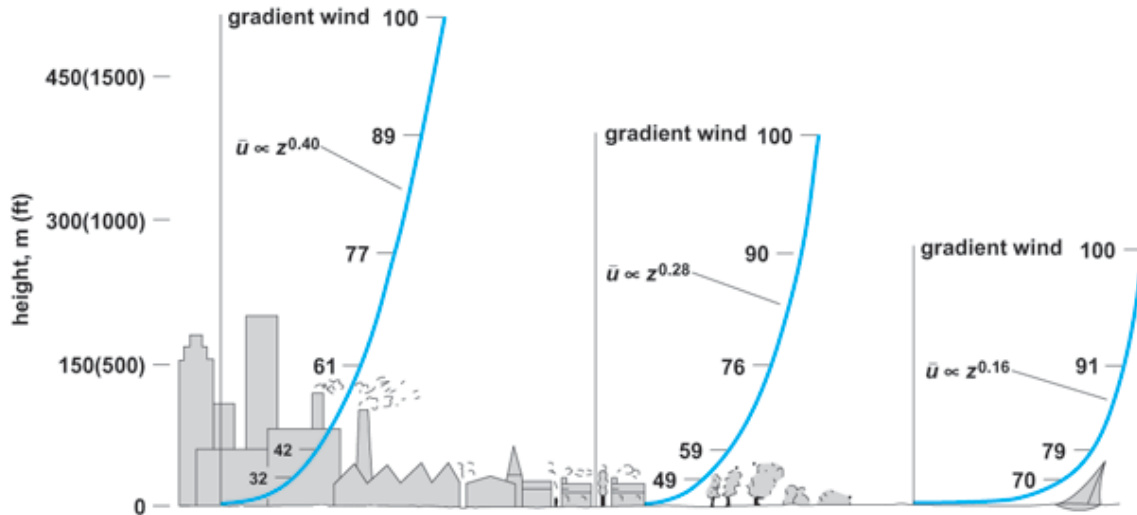
Figure 1.1: Wind speed profile [7].

Since wind turbines can only reach a few tens of meters, most of the available wind energy remains unexplored. Even though wind turbines are still being increased in size, further increasing it begins to present itself as an impracticable solution due to their already high cost. Thus, in order to harvest such high altitude winds, it becomes necessary to develop more efficient solutions without increasing the production costs.

By using a kite connected through a tether instead of a huge tower it is possible to reach those high altitude winds with an incredible save in cost and materials. As the structure of Airborne Wind Energy Systems (AWES) is expected to be much lighter, cheaper and easier to install than conventional wind turbines, these systems have become one of the most promising proposals to generate electrical power at high altitudes.

1.3   Objectives

This dissertation main goals are the design of kite controllers and follow path algorithms, in order to maximize the power output. This is done using Matlab Simulink software.

To do so, the following objectives are considered:

1. Review technologies and principles of high wind power extraction

2. Study of the kite dynamical model

3. Development of a kite simulation platform

4. Design kite controllers

5. Develop path follow algorithms

1.4 Document Structure

Besides this introduction chapter, this thesis has 6 more chapters, organized as follows. In Chapter 2 we introduce Airborne Wind Energy Systems and the different concepts of these systems. In Chapter 3, we describe the model used for the kite power system. In Chapter 4 we do some simulations in order to verify the model. In Chapter 5, we develop a trajectory controller to follow a desired path, and a new strategy to handle wind gusts. In Chapter 6, another trajectory controller is developed based on a nonlinear guidance logic [8]. Also, a Lyapunov stability analysis is provided. In Chapter 7 we summarize the conclusions and suggest some future work.

Chapter 2

Airborne Wind Energy Systems

In this chapter we introduce the main idea of Airborne Wind Energy Systems. We also classify the different AWES concepts according to the way of producing energy and their type of wing. Then, we present some prototypes from the main companies working on AWES. In the last section we do a small discussion.

2.1   Introduction to the Crosswind Kite Power

Back in 1980, Miles L. Loyd proposed what has become one of the most famous ideas of exploring wind energy at high altitudes [1]. His concept was very simple: a kite, or airplane, connected to the ground with a tether, flying on circular trajectories in the sky. A huge power amount can potentially be harvested from these systems since the wind speeds grow fast with height and the aerodynamic lift force $\vec{\mathrm{F}}^{\mathrm{lift}}$ increases with the square of the apparent wind speed v_a [5],

$$\vec{\mathrm{F}}^{\mathrm{lift}} = \frac{1}{2}\rho A c_L v_a^2. \tag{2.1}$$

Thus, the maximum power extraction is obtained when the kite flies at high speeds in a direction perpendicular to the direction of the wind, this is, in crosswind direction.

Two different approaches were described by Loyd, that he called lift mode and drag mode, respectively [1]. The first one uses the tether tension to produce the motion of a generator on the ground, while the later takes advantage of the high apparent wind speed to drive small wind turbines on the kite. In Section 2.2 these concepts are described in detail.

In [1], Loyd also estimated the power output that can be generated with these systems, although under idealized assumptions, which is approximately given by

$$P = \frac{2}{27}\rho A v_w^3 c_L \left(\frac{c_L}{c_D}\right)^2. \tag{2.2}$$

The power output is proportional to the square of the lift-to-drag ratio c_L/c_D, making the wing shape an important aspect for the AWES.
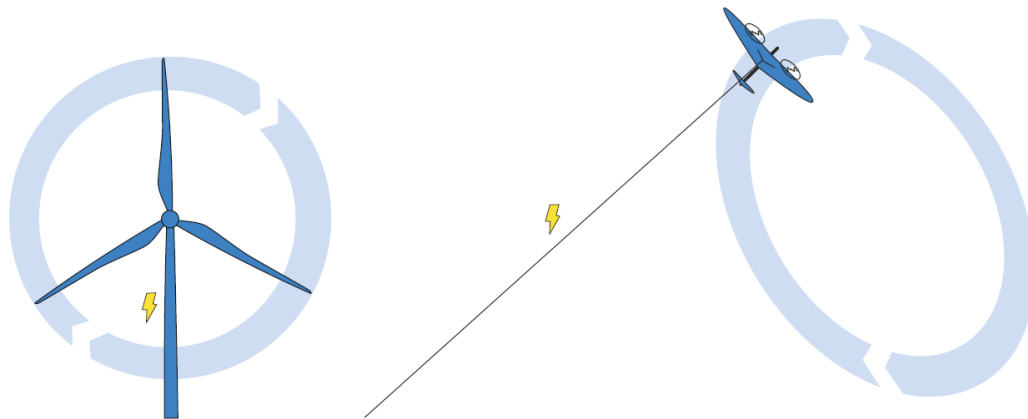
Figure 2.1: AWE systems replace the tips of a wind turbine (left) with a tethered fast flying wing (right, operating in drag mode). Illustration by R. Paelinck [5].

It is unavoidable to compare AWES with wind turbines, as they are the main technology for wind power. While a conventional wind turbine requires large blades and also huge towers and foundations to support them, more than half of the total power output comes from the outer 30% of the blades [5]. The idea of AWES, represented on Figure 2.1, is to replace the tower and the inner parts of the blades with a tether, reducing the amount of materials used.

On the other hand, while a wind turbine is stationary and can be stopped almost immediately in case of a problem, an AWES cannot simply be stopped mid-air. Thus, for safety reasons, these systems need advanced control systems that, whenever the system is not working as intended, can land without major damage.

There are many different Airborne Wind Energy Systems concepts which we will address in the following sections.

2.2 Classification of Airborne Wind Energy Systems

An Airborne Wind Energy System is the whole structure used to convert the kinetic energy of the wind into electrical energy [9]. Generally they can be divided in two parts, a ground station and an aircraft, that are physically connected through a tether. There is a wide variety of AWES concepts, which can be classified according to how energy is produced and their type of wings. Usually, when referring to energy production, we can distinguish two types of AWES: Ground Generation (GG) Systems and Fly Generation (FG) Systems. As the name suggests, in a GG system the conversion of mechanical energy into electrical is done on a ground station while in a FG system such conversion is done on the aircraft (see Figure 2.2). Regarding the type of wing, they can be divided in flexible or rigid wings.

Figure 2.2: Example of Ground-Gen (a) and Fly-Gen (b) AWESs [9].

2.2.1 Ground-Gen Airborne Wind Energy Systems

In a Ground-Gen Airborne Wind Energy System (GG-AWES), or lift mode according to Loyd, electrical energy is produced on the ground. The system uses the strong tether tension to unroll the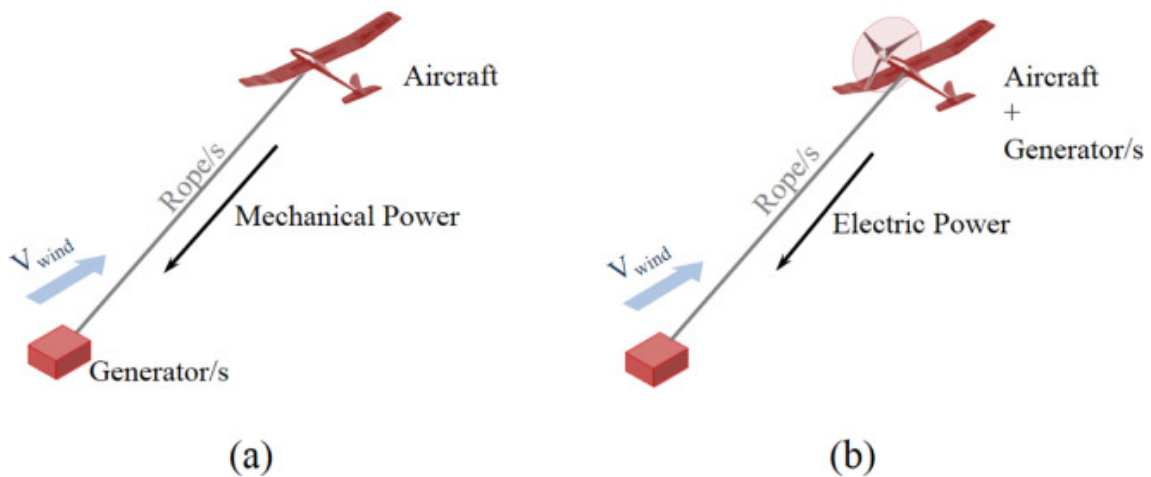 tether from a drum, producing the motion of an electrical generator. In these systems, a complete production cycle consists in two phases (see Figure 2.3).

In the first phase, called generation phase (or *reel-out* phase), the aircraft is controlled in a way to produce a high lift force which, consequently, induces a high tether force, unwinding the tether and inducing the rotation of an electrical generator. During this phase, the aircraft flies mostly in crosswind flight, as it leads to a strong apparent wind velocity and consequently increases the tether force. The path is usually periodic, with the most common being circular or eight-shaped paths.

Since the tether length is finite, a second phase is necessary, generally called recovery phase (or *reel-in* phase), in which the tether is retracted by a motor and the aircraft is set back to its original position. During this phase, the flight path is changed to one that produces less lifting force, in order to minimize the energy spent.

For these systems to be effective, the energy produced in the generation phase has to be larger than the energy consumed in the recovery phase, which should be guaranteed by the control system by adapting the flight paths.

2.2.2 Fly-Gen Airborne Wind Energy Systems

In a Fly-Gen Airborne Wind Energy System (FG-AWES), the aircraft carries one or more wind turbines that produce electrical energy on-board. The turbines add extra drag to the aircraft, so Loyd called this *drag mode*. Energy produced is then transmitted to the ground through a tether that has to both conduct electricity and resist to strong tensions. In this mode energy production is usually continuous, as a recovery phase is not needed.

Many different concepts of FG-AWES have been proposed, as can be seen in Figure 2.4.
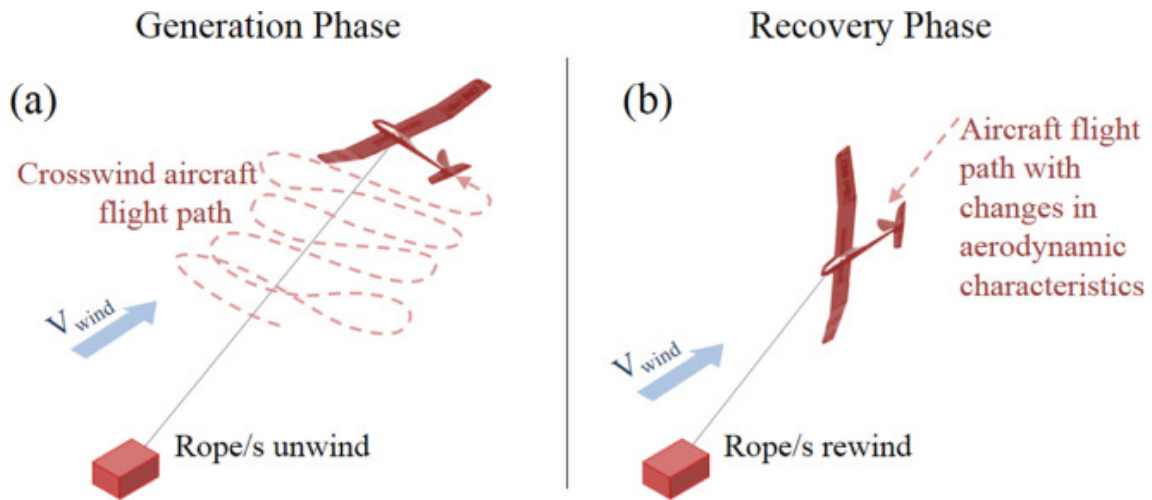
Figure 2.3: Scheme of the two-phase discontinuous energy production for GG-AWESs. a) The energy generation phase occurs during the unwinding of the ropes as the aircraft performs a crosswind flight. b) The recovery phase is performed in order to minimize the energy consumed for the recovery [9].
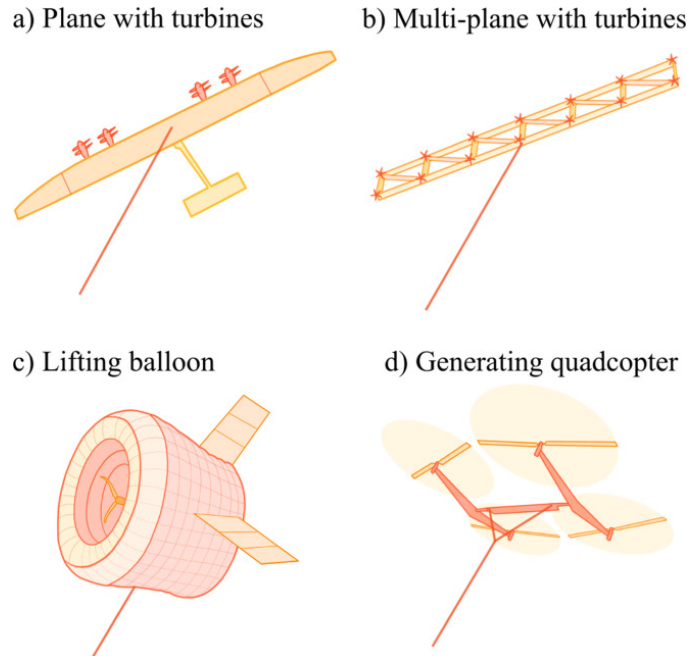
Figure 2.4: Different types of aircraft in Fly-Gen systems. (a) Plane with four turbines, design by Makani Power; (b) Aircraft composed by a frame of wings and turbines, design by Joby Energy; (c) Toroidal lifting aerostat with a wind turbine in the center, design by Altaeros Energies; (d) Static suspension quadrotor in autorotation, design by Sky WindPower [10].

2.2.3 Flexible and Rigid Wings

AWES can also be divided according to their type of wings. These can be flexible, which look like surf kites, or rigid, that are similar to airplanes. Both have their advantages and disadvantages, and its not clearly which option is the best.

Systems with flexible wings can be lightweight, and, in case of a crash, they generally do not cause considerable damage. However they typically fly at moderate speeds and cannot always maintain their shape. On the other hand, systems with rigid wings can always maintain their shape, which makes it easier to control, and can reach very high velocities due to their higher lift to drag ratio, leading to stronger lift forces and subsequently higher power output. Systems with this type of wing are usually heavier, and in case of a crash they may be more dangerous.

2.2.4 Multiple Wing Systems

To reach high altitude winds, a long tether is necessary, however, a long tether also induces a high tether drag, which is significant on these systems. So, in order to fight this drawback, some concepts use multiple kites and introduce two kinds of tether. A long primary tether allows the AWES to reach high altitudes, while shorter secondary tethers connect the primary tether to the kites (see Figure 2.5). This way, the primary tether movement is almost none, as the kites flies in loops around the attachment point between the two tethers, reducing significantly the tether drag losses [11].

Another concept using multiple wings is based on the *laddermill*, presented by W. Ockels [12], which uses one main tether with several kites attached vertically. Theoretically, this idea allows for creating a large scale system using several small kites instead of a large one.

The main problem with multiple wing systems is that interconnected wings are not reliable and are very hard to control. The take-off and landing of these systems is also very delicate, so no large scale AWES with multiple kites has been built yet.

2.2.5 Lighter than Air Systems

The majority of Airborne Wind Energy Systems stay airborne thanks to aerodynamic lift. There are however a few systems in which the airborne part is lighter than air, allowing them to stay static in the air.

These systems usually need a large volume, generally filled with Helium, to compensate for the weight of the system. The advantage of lighter than air systems is that they can stay airborne even when there is no wind, and the take-off and landing of such systems are usually more simple.
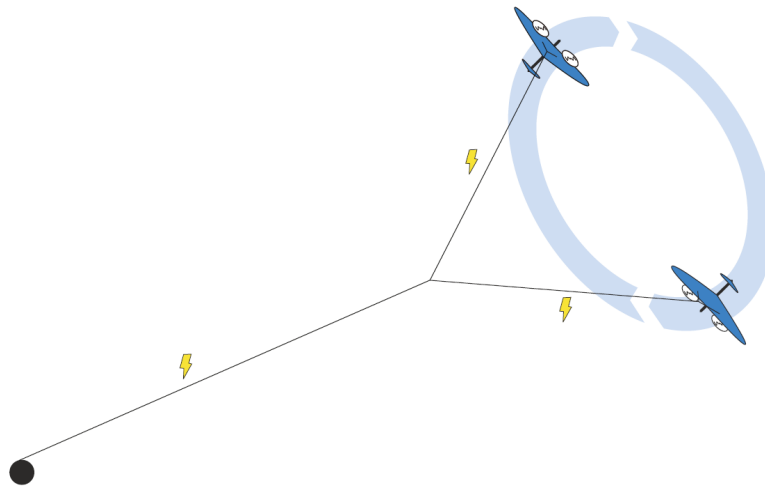
Figure 2.5: Visualization of a dual airplane system with reduced tether drag. Illustration by R. Paelinck [5].

2.3 AWES Prototypes

As seen in the previous sections, there is a wide variety of AWES concepts, and companies and university groups take different approaches when developing their systems, either in the way energy is produced, the type of kite used or the way the kite is steered. In this section, some prototypes are presented.

Ground-Gen AWES

Many different prototypes of GG-AWES have been developed by companies. One example is KitePower [13], founded as a spin-off from the research group at TU Delft, that uses an inflatable flexible wing kite with a main tether, and an airborne control pod to control the length of the steering lines [14]. They are currently developing a 100kW prototype (see Figure 2.6).

(a)

(b)

Figure 2.6: (a) TU Delft inflatable flexible wing kite; [13] (b) KitePower 100kW ground station [15].

Still using flexible wings, there are other companies like KiteGen [16] or Enerkite [17], that instead use a ground control pod for steering, which eliminates additional drag and weight [18]. Their systems use two or three main tethers, and steer the kite by adjusting the length of the tethers [19].

Using rigid wings we have, for example, AmpyxPower [20], a Dutch company founded in 2008. After the AP-2 (see Figure 2.7a), which was a 20kW system, the company is now developing the AP-3 (under construction) and the AP-4 (still in design phase). The AP-3 is a 250kW system and uses an aircraft with a wingspan of 12m and weights 375kg (see Figure 2.7b). The plan for the AP-4 is for it to be a 2MW system.

(a)   (b)

Figure 2.7: Ampyx Power prototypes. (a) AP-2 20kW prototype during a free gliding flight; (b) Rendering of the AP-3 aircraft [20].

Another company developing a rigid wing prototype is TwingTec [21]. The Swiss company is currently developing a 100kW prototype, the TT100, which has a wingspan of 15m (see Figure 2.8). Even though this prototype is a GG system, its wings have rotors that are used for autonomous take-off and landing. This system can be integrated into a container, allowing for low cost transportation and easy installation, even in remote areas.

Figure 2.8: Example of a GG-AWES, by TwingTec [21].

Still on the GG systems but on a completely different concept is the Portuguese company Omnidea [22], which does not use crosswind power. Instead, their prototype uses cylinders filled

Figure 2.9: Omnidea prototype.

with helium and exploits the Magnus effect to move up and down (see Figure 2.9).

Fly-Gen AWES

The most famous company using FG systems is Makani Power [23], a company from California founded in 2006 that was acquired by Google in 2013. They are currently developing a 600kW prototype, the "M600". This FG prototype has rigid wings, eight wind turbines and a wingspan of 28m. The turbines work as motors for a vertical take-off and landing of the aircraft, and as generators when the kite transitions into crosswind flight.

Figure 2.10: Makani Power System [23].

Some companies use FG systems but do not exploit crosswind motion. One example is Sky WindPower, which uses a quadcopter with rotors for power generation. The rotors are used as motors to reach high altitudes, and when at a certain altitude, the frame is inclined and the rotors start working as generators. A representation of this system is done in figure 2.4d.

Another concept of FG systems is lighter than air systems, with prototypes being developed by Altaeros Energies [24] and Magenn Power [25]. The first uses a balloon filled with Helium, that surrounds the turbine on the center (see Figure 2.11a). Magenn uses a large horizontally rotating drum filled with Helium to generate power (see Figure 2.11b).

(a)   (b)

Figure 2.11: Lighter than air systems. (a) Altaeros prototype [24]; (b) Magenn Power concept [25].

2.4   Discussion

In this chapter we presented the concept of Airborne Wind Energy Systems, and the different ideas to generate power at high altitudes. The main difference between these systems is the type of kite used and the generator placement.

A ground generator allows for, usually, lighter airborne systems, however, energy is produced by unrolling a tether, and since the cable length is finite, energy production is not continuous and a reel-in phase is necessary. FG systems on the other hand can produce continuously, but since the generators are in the air, these systems are generally heavier. Some of these systems use the turbines as motors for the take-off and landing maneuvers, like Makani Power [23] for example. With every system having its advantages and disadvantages, it is not clear which one is the best.

Although, ever since Loyd's first idea, many concept variants have been proposed, it is only after the development over the last few years, in both materials and technology, that these systems are starting to become a reality and approaching economic competitiveness, and consequently attracting companies to invest in them. In December 2016, E.ON, Schlumberger and Shell Technology Ventures funded the British AWES company Kite Power Systems with £5 million (€ 5.86 m) [26]. In April 2017, Ampyx Power and E.ON have entered into a cooperation aiming to develop Ampyx Power technology into commercial deployment [27].

Chapter 3

Dynamical Model of the Kite Power System

In this chapter we describe the Kite Power System Dynamical Model. We start by detailing the different coordinate systems and then the acting forces on the kite. After that, we describe the control variables and their influence in the kite's behaviour.

3.1 Coordinate system

The forces acting on the kite are modelled in a spherical coordinate system positioned at the center of mass of the kite, similarly to what was done in [28, 29]. Three coordinate systems are considered:

Global G: An inertial Cartesian coordinate system (x, y, z) whose the origin is on the ground at the point of attachment of the tether. A basis of this coordinate system is $(\vec{\mathbf{e}}_x, \vec{\mathbf{e}}_y, \vec{\mathbf{e}}_z)$. We consider that x is aligned according to the wind direction $\mathbf{v}_w = (v_w, 0, 0)$.

Local L: A non-inertial spherical coordinate system (r, ϕ, β). A basis of this coordinate system is $(\vec{\mathbf{e}}_r, \vec{\mathbf{e}}_\phi, \vec{\mathbf{e}}_\beta)$ (Fig. 3.1).

Body B: A non-inertial Cartesian coordinate system attached to the kite body. A basis of this coordinate system is $(\vec{\mathbf{e}}_1, \vec{\mathbf{e}}_2, \vec{\mathbf{e}}_3)$. Consider $\vec{\mathbf{e}}_1$ coincides with the kite longitudinal axis pointing forward, $\vec{\mathbf{e}}_2$ coincides with the kite transversal axis pointing to the left wing tip, and $\vec{\mathbf{e}}_3$ with the kite vertical axis pointing upwards (Fig. 3.2).

Considering the position of the kite in the G-coordinate system

$$\mathbf{p} = \begin{bmatrix} x \\ y \\ z \end{bmatrix} = \begin{bmatrix} r\cos(\beta)\cos(\phi) \\ r\cos(\beta)\sin(\phi) \\ r\sin(\beta) \end{bmatrix},$$
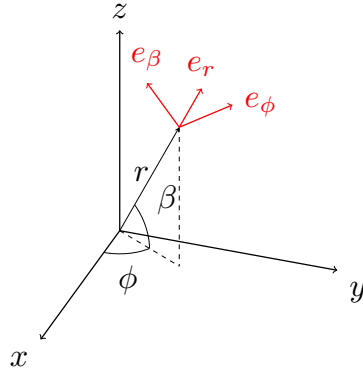
Figure 3.1: Global and Local coordinate systems [28].

the rotation matrix from L-coordinate system to G-coordinate system is

$$
\mathrm{R_{LG}} = \begin{bmatrix} \vec{\mathbf{e}}_r & \vec{\mathbf{e}}_\phi & \vec{\mathbf{e}}_\beta \end{bmatrix} = \begin{bmatrix} \cos(\beta)\cos(\phi) & -\sin(\phi) & -\sin(\beta)\cos(\phi) \\ \cos(\beta)\sin(\phi) & \cos(\phi) & -\sin(\beta)\sin(\phi) \\ \sin(\beta) & 0 & \cos(\beta) \end{bmatrix},
$$

This is an orthogonal matrix, so the rotation from G coordinate system to L is

$$
\mathrm{R_{GL}} = \mathrm{R_{LG}^{-1}} = \mathrm{R_{LG}^{\top}}.
$$

Considering the apparent wind velocity

$$
\mathbf{v}_a = \mathbf{v}_w - \dot{\mathbf{p}},
$$

we assume that its radial component $\mathbf{v}_{a,r}$ is always strictly positive. Also, we consider that the kite body longitudinal axis is at all times aligned with the apparent wind velocity, that is

$$
\vec{\mathbf{e}}_1 = -\frac{\mathbf{v}_a}{\|\mathbf{v}_a\|}.
$$

Consider the local tangent plane τ, which is tangent to a sphere centred at the origin and contains axis $\vec{\mathbf{e}}_\phi$ and $\vec{\mathbf{e}}_\beta$. Let ψ be the roll angle measuring the rotation around the longitudinal
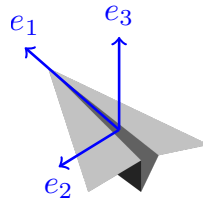

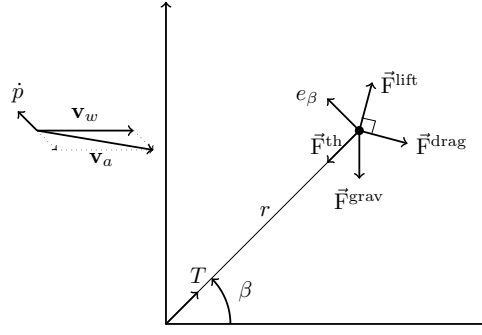Figure 3.2: Body coordinate system [28].

Figure 3.3: Forces acting on the kite [28]

axis ($\vec{\mathbf{e}}_1$). We consider that initially, for $\psi = 0$, $\vec{\mathbf{e}}_2$ is in the plane τ. Then, we define $\tilde{e}_2$ as the "unrotated" axis, this is, $\tilde{e}_2 = \vec{\mathbf{e}}_2$ when $\psi = 0$. Therefore, we have that $\tilde{e}_2 \perp \vec{\mathbf{e}}_r$, and $\tilde{e}_2 \perp \vec{\mathbf{e}}_1$. Thus, we can then define $\tilde{e}_2 = \dfrac{\vec{\mathbf{e}}_r \times \vec{\mathbf{e}}_1}{\|\vec{\mathbf{e}}_r \times \vec{\mathbf{e}}_1\|}$.

Finally, we assume that the roll angle ψ around $\vec{\mathbf{e}}_1$ can be controlled directly. Using Rodrigues' formula to rotate $\tilde{e}_2$ by ψ around $\vec{\mathbf{e}}_1$, we obtain

$$\vec{\mathbf{e}}_2 = \tilde{e}_2 \cos\psi + (\vec{\mathbf{e}}_1 \times \tilde{e}_2)\sin\psi + \vec{\mathbf{e}}_1(\vec{\mathbf{e}}_1 \cdot \tilde{e}_2)(1 - \cos\psi)$$

and finally, we define $\vec{\mathbf{e}}_3$ to be $\vec{\mathbf{e}}_3 = \vec{\mathbf{e}}_1 \times \vec{\mathbf{e}}_2$.

3.2   Acting Forces

Considering the kite position (**p**) and its mass (m), the total force acting on the kite can be decomposed into the tether force, gravity force and aerodynamical force, where the last can be divided into its lift and drag components (see Fig. 3.3).

Thus, we have that

$$m\ddot{\mathbf{p}} = \vec{\mathrm{F}}^{\text{th}} + \vec{\mathrm{F}}^{\text{grav}} + \vec{\mathrm{F}}^{\text{aer}}(\alpha) \tag{3.1}$$

where

$$\vec{\mathrm{F}}^{\text{th}} = -T\,\vec{\mathbf{e}}_r = \begin{bmatrix} -T \\ 0 \\ 0 \end{bmatrix}_{\text{L}},$$

$$\vec{\mathrm{F}}^{\text{grav}} = -mg\,\vec{\mathbf{e}}_z = \begin{bmatrix} 0 \\ 0 \\ -mg \end{bmatrix}_{\text{G}} = \begin{bmatrix} -mg\,\sin\beta \\ 0 \\ -mg\,\cos\beta \end{bmatrix}_{\text{L}},$$

$$\vec{\mathrm{F}}^{\text{aer}}(\alpha) = \vec{\mathrm{F}}^{\text{lift}}(\alpha) + \vec{\mathrm{F}}^{\text{drag}}(\alpha),$$

and

$$\vec{F}^{\text{lift}}(\alpha) = {}^1\!/\!{}_2\rho A c_{\text{L}}(\alpha)\|\mathbf{v}_a\|^2\vec{e}_3,$$

$$\vec{F}^{\text{drag}}(\alpha) = {}^1\!/\!{}_2\rho A c_{\text{D}}(\alpha)\|\mathbf{v}_a\|^2\vec{e}_1.$$

Therefore

$$\vec{F}^{\text{aer}}(\alpha) = {}^1\!/\!{}_2\rho A\|\mathbf{v}_a\|^2(c_{\text{L}}(\alpha)\vec{e}_3 - c_{\text{D}}(\alpha)\vec{e}_1).$$

Considering the L-coordinate system, we have that

$$\ddot{\mathbf{p}} = \begin{bmatrix} \ddot{r} \\ r\ddot{\phi}\cos(\beta) \\ r\ddot{\beta} \end{bmatrix}_{\text{L}} + \underbrace{\begin{bmatrix} -r\dot{\beta}^2 - r\dot{\phi}^2\cos^2(\beta) \\ 2\dot{r}\dot{\phi}\cos(\beta) - 2r\dot{\phi}\dot{\beta}\sin(\beta) \\ 2\dot{r}\dot{\beta} + r\dot{\phi}^2\cos(\beta)\sin(\beta) \end{bmatrix}_{\text{L}}}_{-{}^1\!/\!{}_m\vec{F}^{\text{inert}}} \tag{3.2}$$

where the second term is $-{}^1\!/\!{}_m\vec{F}^{\text{inert}}$. $\vec{F}^{\text{inert}}$ represents the inertial forces acting on the kite (centrifugal and Coriolis), in the L-coordinate system.

Denoting the total resulting force by F, we can write

$$F = m \begin{bmatrix} \ddot{r} \\ r\ddot{\phi}\cos(\beta) \\ r\ddot{\beta} \end{bmatrix} = \vec{F}^{\text{th}} + \vec{F}^{\text{grav}} + \vec{F}^{\text{aer}}(\alpha) + \vec{F}^{\text{inert}}. \tag{3.3}$$

We assume that the tether acceleration $\ddot{r}$ can be controlled directly by a_t, and designate T as the tether tension at the base. Now, we can write $T = F_r - ma_t$. Defining the state $\mathbf{x} = \left(r, \phi, \beta, \dot{r}, \dot{\phi}, \dot{\beta}\right)$ and the control $\mathbf{u} = (a_t, \alpha, \psi)$, the dynamic equation is

$$\dot{\mathbf{x}}(t) = f(\mathbf{x}(t), \mathbf{u}(t)) = \frac{\text{d}}{\text{d}t}\begin{bmatrix} r \\ \phi \\ \beta \\ \dot{r} \\ \dot{\phi} \\ \dot{\beta} \end{bmatrix} = \begin{bmatrix} \dot{r} \\ \dot{\phi} \\ \dot{\beta} \\ a_t \\ \dfrac{1}{mr\cos(\beta)}F_\phi \\ \dfrac{1}{mr}F_\beta \end{bmatrix}.$$

3.3 Control Variables

3.3.1 Tether Acceleration

The tether acceleration is the control variable that allow us to control the tether reel-in and reel-out movement. It is known that the maximum power output is obtained when the kite unrolls at about one-third of the wind velocity [5], that is

$$v_{reel\_out} \approx \frac{1}{3} v_w. \tag{3.4}$$

Thus, in the production phase, since our objective is to maximize the power output, we want to control the tether acceleration in order to obtain the required reel-out speed.

In the recovery phase, we have to find a balance between time and energy consumption. While a fast reel-in speed is less time not producing, it also lead to a bigger energy consumption and a possible loss of control of the kite. On the other hand, a slow reel-in speed, even though the energy consumption is much smaller, it is time where energy is not being produced, making the system not efficient. Therefore, a balance has to be found between time and energy consumption when determining the reel-in velocity.

3.3.2 Angle of Attack

The angle of attack is the angle between the kite wing chord and the apparent wind velocity (see Figure 3.4). The lift and drag coefficients, c_L and c_D, varies with the angle of attack. Increasing the angle of attack usually increases the lift coefficient up to a certain maximum c_L, after which it starts decreasing. Thus, when in production phase, we want to control the angle of attack α in order to obtain a high lift force, which leads to a high tether force and consequently to a bigger power output. The opposite happens in the recovery phase, where we want the minimal lift force while retrieving the kite, therefore, a small angle of attack.
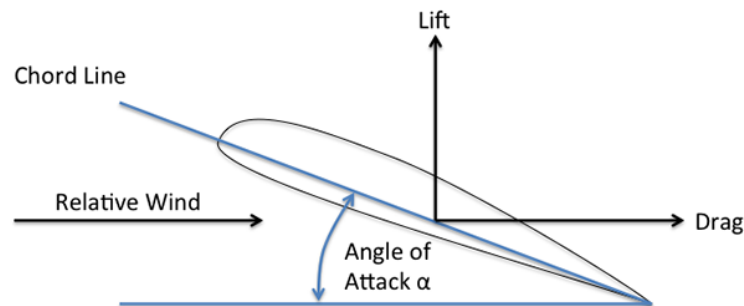

Figure 3.4: Angle of Attack [30].

3.3.3   Roll Angle

As seen before, the roll angle ψ is the kite's rotation around $\vec{e}_1$, which is the kite longitudinal axis. This is the main control variable for the heading direction of the kite.

Considering a two line kite where d is the distance between attachment points and Δr is the relative difference between the lengths of each line, we have $\sin \psi = \Delta r / d$ (see Fig. 3.5).
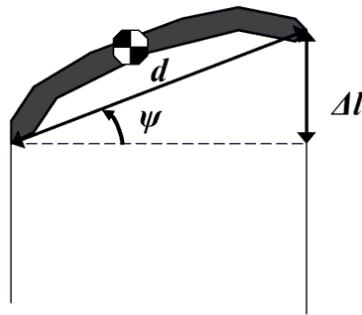
Figure 3.5: Roll angle ψ [29].

In a rigid wing kite, the roll angle can also be controlled by acting on the wing ailerons.

Chapter 4

2D Simulations of a Kite Power System

In this chapter we do simulations with simplifications the kite model presented in Chapter 3. We start by the Underwater Kite problem, a 2D problem in the horizontal plane, that is, with $\beta = 0$, and then we address the Airborne KPS problem in 2D in the vertical plane $\phi = 0$. For each case, we build the model in Simulink and do some simulations in order to verify the model and to gain sensitivity to the problem. Finally, we simulate the $\phi = 0$ system to find the relation of the kite elevation angle with the wind velocity and the angle of attack, as well as its equilibrium elevation.

4.1 Underwater Kite Power System

We start by presenting the Underwater Kite Power System [31]. The principle is the same as the AWES, the only difference is that the fluid is now water. While the velocities on water are generally much lower than on air, the fact that the fluid density ρ is more than 800 times higher on water compensates for it.

We address this as a 2D problem in the horizontal plane, so we consider the elevation angle $\beta = 0$ on the model presented above. Also, gravity force is not considered as it is compensated by buoyancy.

For the control, only the tether acceleration (a_t) and the angle of attack (α) are considered. We can think of this system as a boat rudder, where the angle of attack is the rudder angle.

4.1.1 Simulation Results

We build the Underwater Kite model in Simulink as can be seen in Figure 4.1. For the Underwater Kite simulations, the parameters considered are the ones presented in Table 4.1. The hydrodynamic coefficients used in simulations are given by (4.1) and (4.2), respectively. We consider this values for small values of α, when the kite is considered to behave as a thin plate [32].
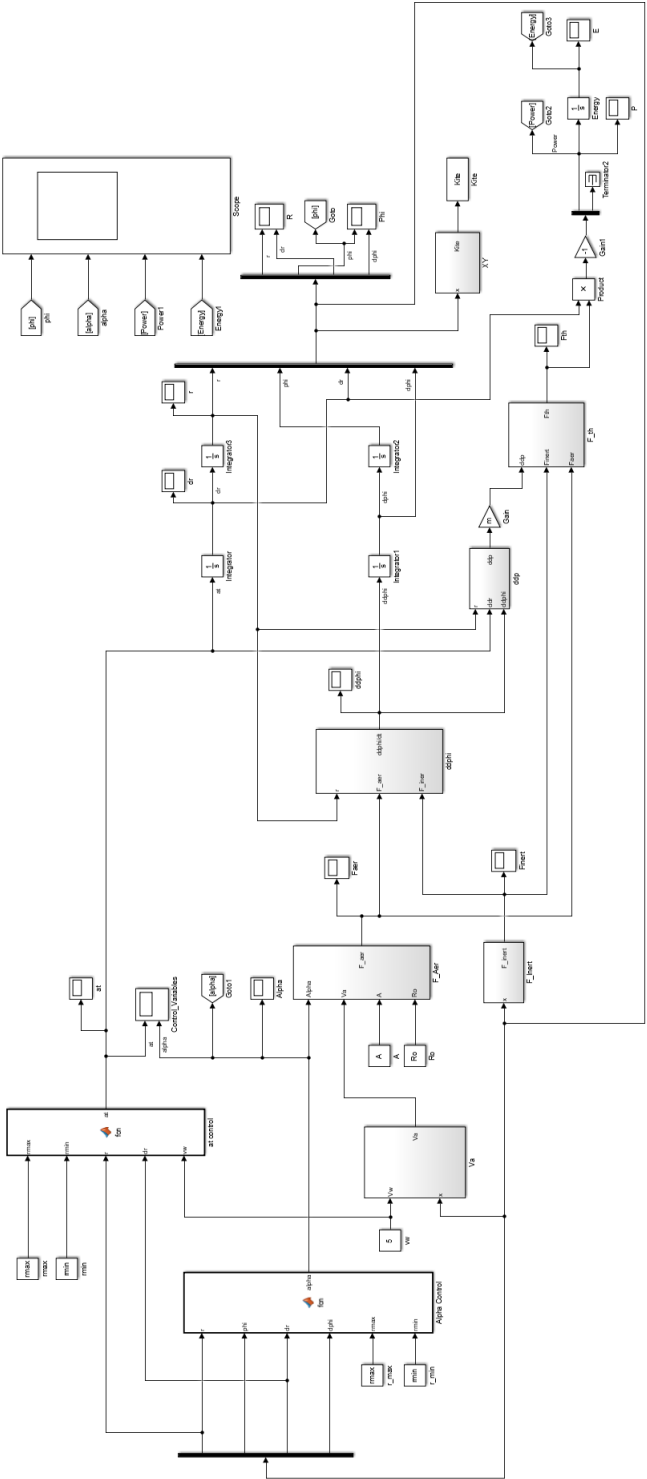
Figure 4.1: Simulink model for the Underwater Kite Power System.

Table 4.1: Underwater Kite Simulation Parameters

Parameter	Value
ρ	$1000\ \mathrm{kg\,m^{-3}}$
v_w	$3\ \mathrm{m\,s^{-1}}$
m	$100\ \mathrm{kg}$
A	$2\ \mathrm{m^2}$
AR	2

$$c_L(\alpha) = \frac{2\pi\alpha}{1 + \frac{2\alpha}{\mathit{AR}}} \tag{4.1}$$

$$c_D(\alpha) = 1.28\sin\alpha + \frac{c_L^2(\alpha)}{0.7\pi\mathit{AR}} \tag{4.2}$$

We simulate the system with the parameters presented above. The kite trajectory is represented in Figure 4.2. We can clearly see the kite production phase and, when $r = r^{max}$, we retract the kite back. The state variables are shown in Figure 4.3 and the control variables in Figure 4.4. The power output and energy are shown in Figure 4.5.

4.1.2 Discussion

The simulation shows successful results in producing electrical power with this device. The kite oscillates in a defined interval $\phi \in [-30; 30]$ degrees during the production phase. As r reaches its maximum length, we center the kite in $\phi = 0$ and set the angle of attack $\alpha = 0$. In this simulation the tether reel-in and reel-out velocities are $1/3v_w$. This is the ideal velocity for production phase, as it maximizes the energy production [5]. In this type of systems the recovery phase is usually much shorter than the production phase, although, in this simulation we use the same speed in both phases. We can see in Figure 4.5 that energy is indeed being produced and, even though the recovery phase duration is not ideal, the energy consumption is almost zero during it. An average power of 50kW (with instant peaks of up to 100kW) was attained, when using a $2m^2$ kite in a water stream of $3ms^{-1}$.

4.2 2D Airborne KPS Problem

Now we address the Airborne Wind Energy System as a simplified 2D problem in the vertical plane $\phi = 0$. The objective of this simulation is to see the influence the angle of attack α has in the elevation angle. Once again, in this simulation the control variables considered are only the tether acceleration (a_t) and the angle of attack (α).
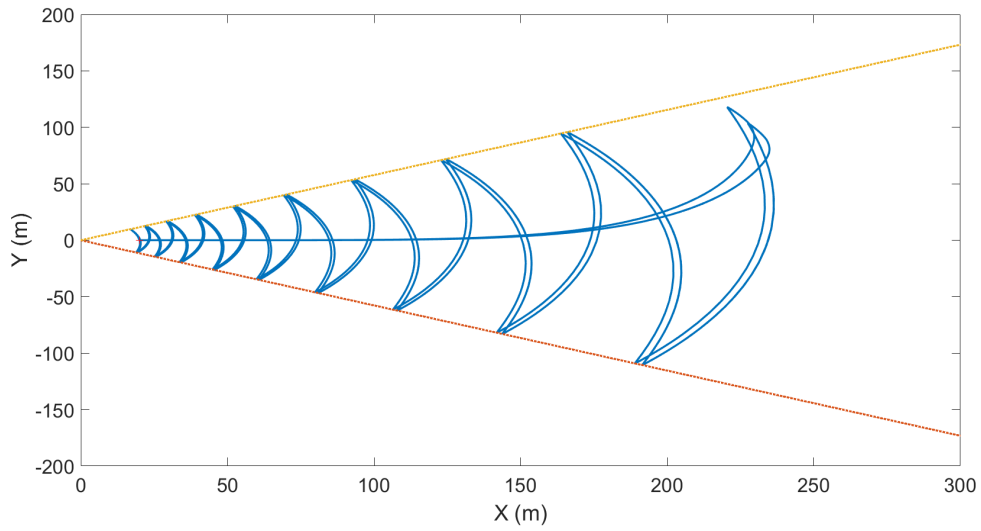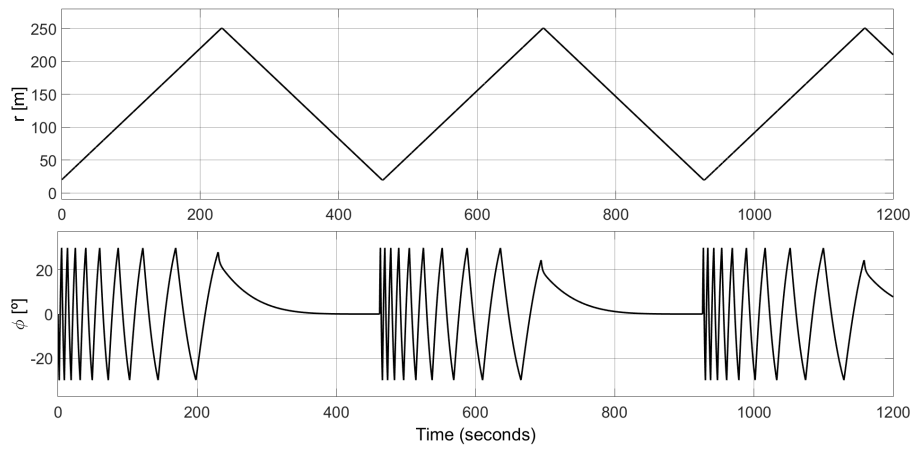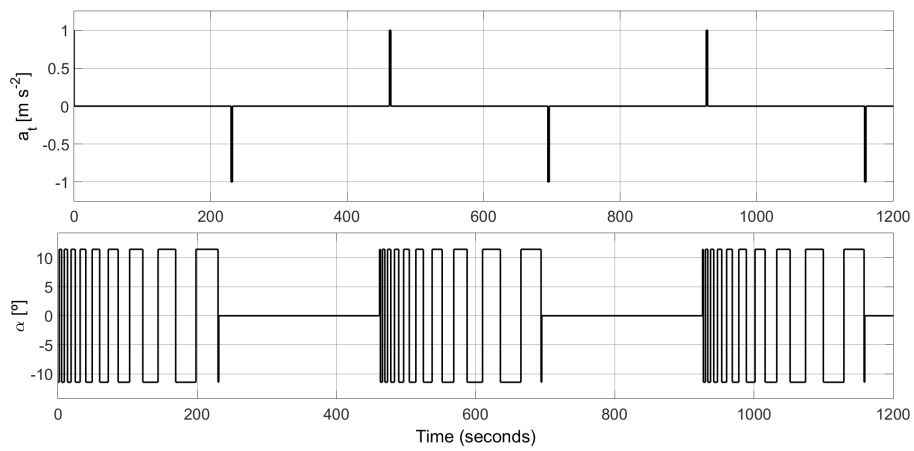
Figure 4.2: Underwater Kite Trajectory.

Figure 4.3: Underwater Kite State Variables (r, ϕ).

Figure 4.4: Underwater Kite Control Variables (a_t, α).
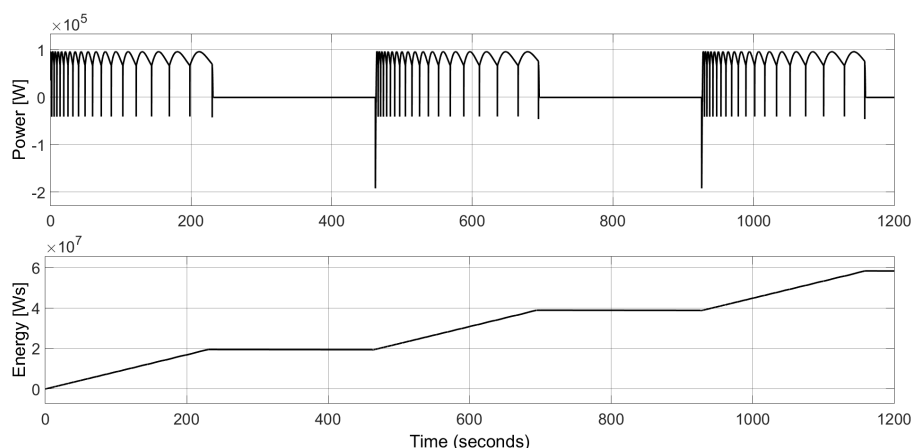
Figure 4.5: Underwater Kite Power and Energy.

4.2.1 Simulations Results

The aerodynamic coefficient values were obtained by using a linear regression from the data in [33]. These are the values used in our simulations:

$$\begin{cases} c_L(\alpha) = 0.3 + 0.1\alpha, & 0 < \alpha < 12 \\ c_L(\alpha) = 9.9 - 0.7\alpha, & 12 < \alpha < 14, \end{cases} \tag{4.3}$$

$$c_D(\alpha) = 0.012 + 0.01\alpha. \tag{4.4}$$

We consider the simulation parameters of the kite system defined in Table 4.2.

Table 4.2: Simulation Parameters

Parameter	Value
ρ	$1.2 \mathrm{\ kg\,m^{-3}}$
v_w	$10 \mathrm{\ m\,s^{-1}}$
g	$9.8 \mathrm{\ m\,s^{-2}}$
m	$0.7 \mathrm{\ kg}$
A	$0.28 \mathrm{\ m^2}$

The 2D Simulink model is presented in Figure 4.6. In Figure 4.7 the kite trajectory is shown. In Figure 4.8 we can see the state variables (r, β). The control variables (a_t, α) are shown in Figure 4.9 and the system power output and energy in Figure 4.10.

4.2.2 Discussion

As before, we define the production phase limits in a interval $\beta \in [20, 60]$ degrees. We can see that the kite surpasses this limits and the reaction to changes in the angle of attack is not immediate. When $r = r^{max}$, we pull the kite back and this time we set the angle of attack α to a higher value. This is necessary to decelerate the kite, as setting α to zero would prompt the kite to fall. Thus,
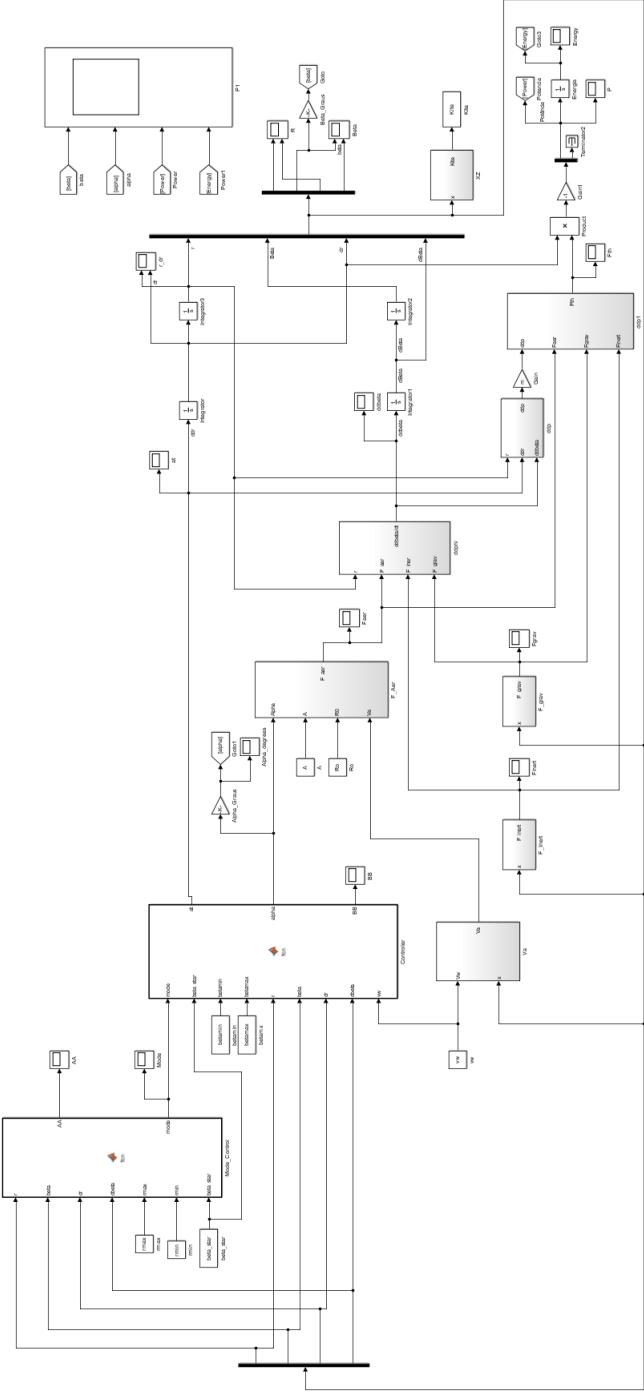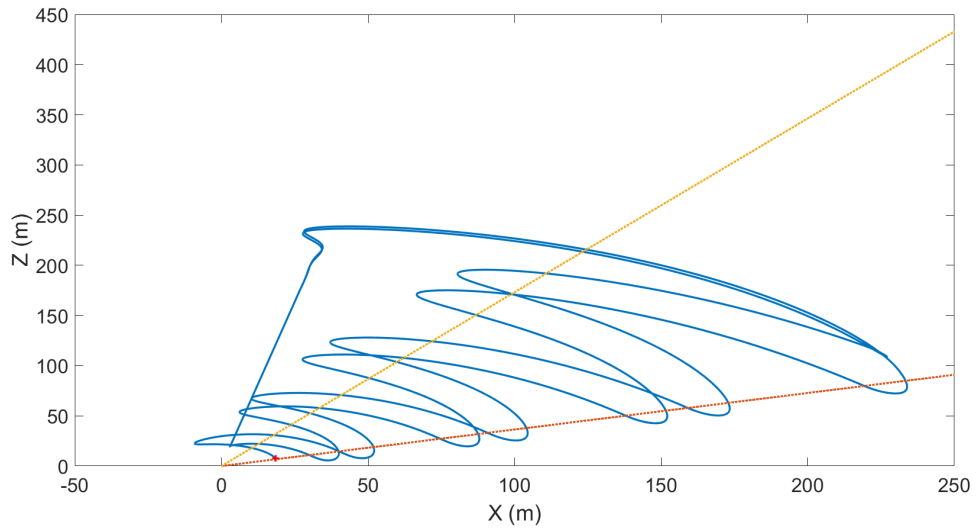
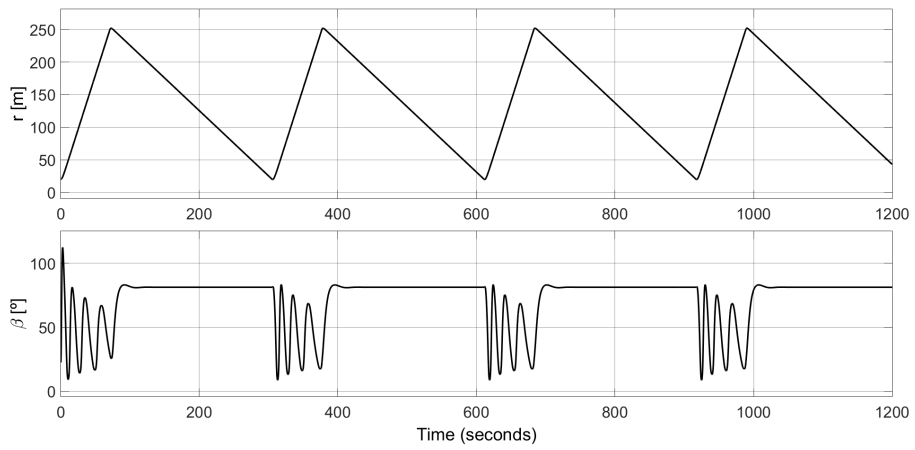Figure 4.6: 2D Kite Simulink Model.

Figure 4.7: 2D Kite Trajectory.

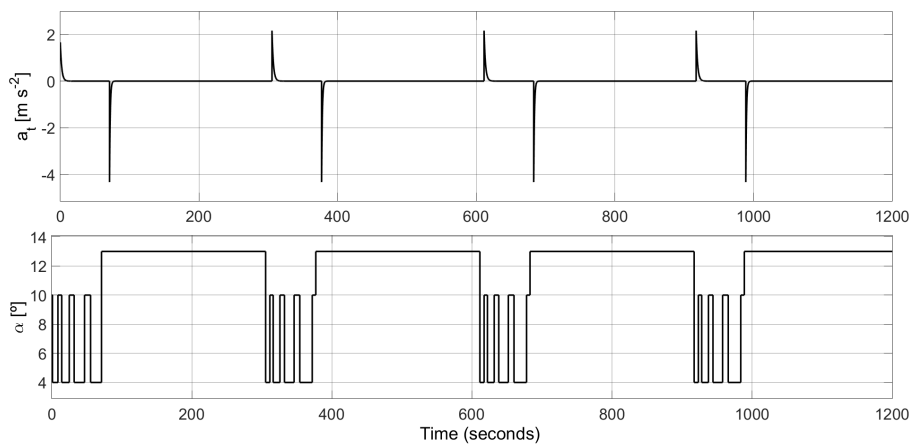Figure 4.8: 2D Kite State Variables (r, β).

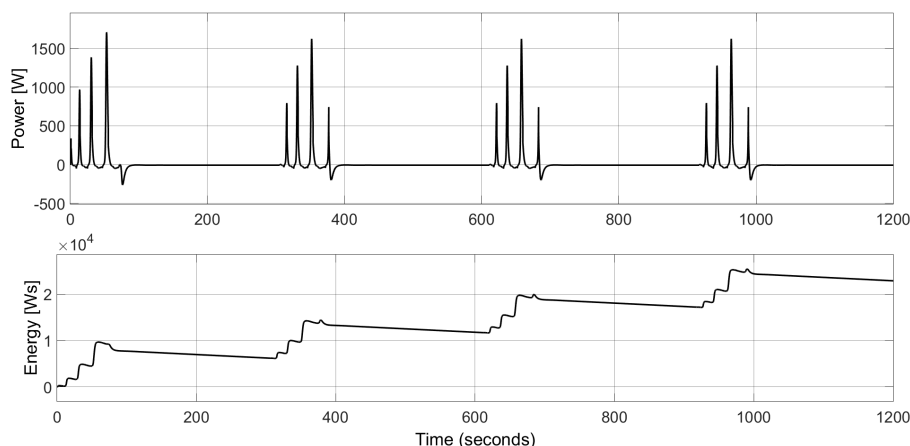Figure 4.9: 2D Kite Control Variables (a_t, α).

Figure 4.10: 2D Kite Power and Energy.

setting α to a high value leads to a small lift force, which is necessary in recovery phase, but also a high drag force, allowing us to stall the kite.

The tether reel-out speed is set to $1/3v_w$, maximizing the energy production, however we could not achieve a fast reel-in speed, as it would make the kite fall. Despite that, we can see in Figure 4.10 that energy is being produced. In this simulation, even though we have attained instant peaks of 1600kW, the average power is only approximately 21W. For this reason, we consider it is not efficient to explore the system using this 2D strategy.

4.3   The Elevation Angle and its relation with Wind Velocity and Angle of Attack

With the parameters defined for the lift and drag coefficients, we made some simulations in order to obtain a relation between the stationary elevation angle β and the wind velocity v_w. We do that by fixing the angle of attack α to a certain value, and simulating the system with wind velocities $v_w \in [0,25]$. The results, for an angle of attack $\alpha = 5^o$, can be seen on Figure 4.11.

We can see that, for low wind velocities, the lift force is not enough to elevate the kite. As the wind velocity value is increased, there is a certain wind velocity where $\vec{F}^{lift} = \vec{F}^{grav}$, from which the kite begins to elevate. After that, and for a wind velocity interval, the kite oscillates between some elevation angles and does not have enough drag to stabilize, so, in this interval, the kite stays oscillating indefinitely. The lines represent the minimum and maximum elevation angle of the kite's oscillation, as well as the average elevation angle.

When reaching a certain strong wind velocity, the kite stabilizes at an equilibrium elevation $\beta^\star$ (this is represented in Figure 4.11 by the dotted red line). The reasons for this to happen are further explained in Section 4.3.1.

We made these simulations with different values of α, to see what influence it had in the elevation angle (see Figure 4.12). We can see that, as we increase the angle of attack (up to a certain maximum), the kite starts elevating with lower wind velocities. This is expected, since
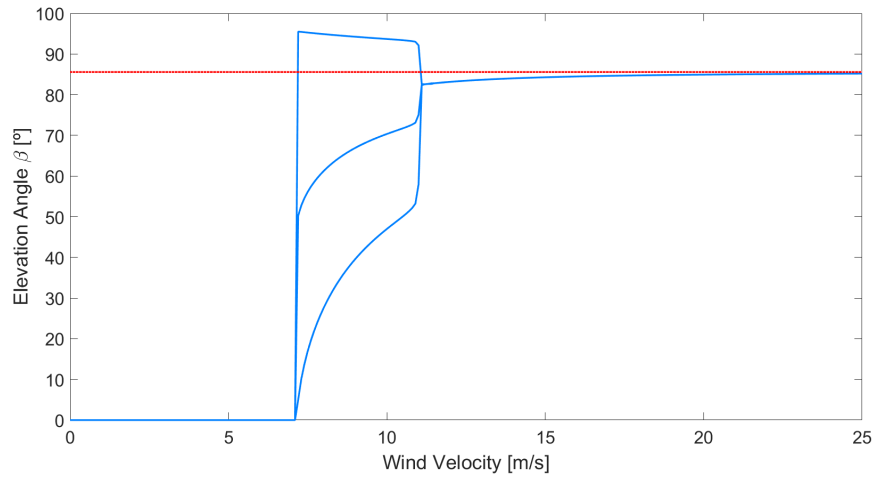
Figure 4.11: Relation between Elevation Angle β and Wind Velocity for $\alpha = 5^o$.

increasing the angle of attack leads to a higher lift force, so we have $\vec{F}^{\text{lift}} = \vec{F}^{\text{grav}}$ with a lower wind velocity. We can also see that the oscillation interval is smaller as we increase α, and that the kite stabilizes with lower values of wind velocity.
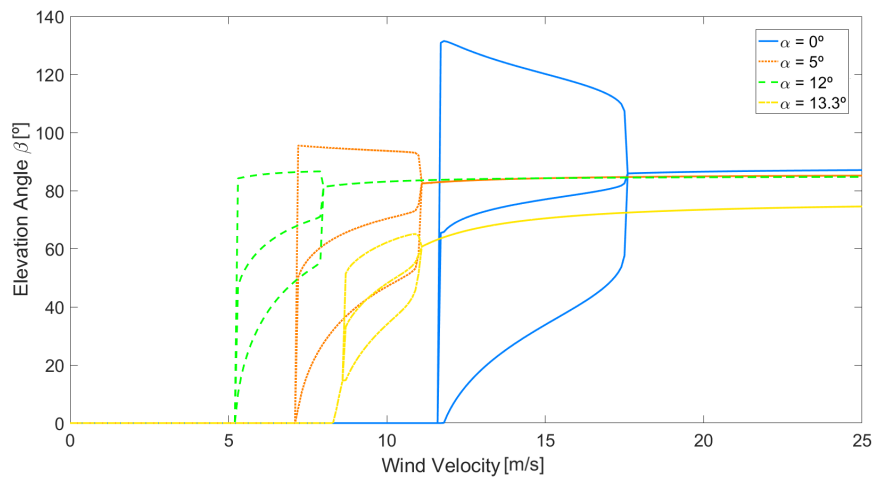
Figure 4.12: Relation between Elevation Angle β and Wind Velocity with different values of α.

4.3.1   Equilibrium Elevation

Consider the case of high values of apparent wind speed, when the aerodynamical lift force is much higher than gravity. This happens either when wind velocities are too strong or when the tether is being recoiled fast.

In such case, we consider

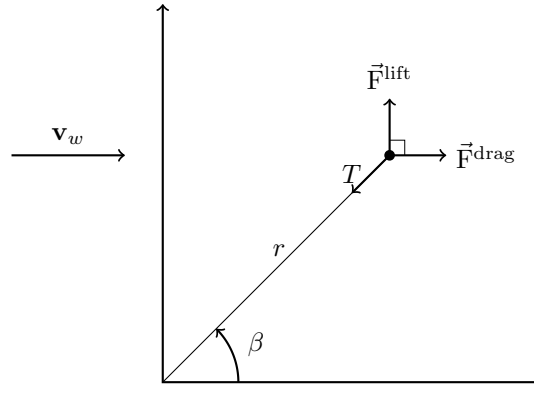$$\vec{T} = \vec{F}^{\text{lift}} + \vec{F}^{\text{drag}}.$$

Figure 4.13: Kite Forces for high values of apparent wind speed and $\dot{r} = 0$.

Then, when the kite is stopped or at very low speeds ($\dot{r} \approx 0$), the drag is aligned with the wind, horizontal, and the lift is vertical (see Figure 4.13).

Therefore,

$$\beta^\star = \arctan\left(\frac{\vec{F}^{\text{lift}}}{\vec{F}^{\text{drag}}}\right) = \arctan\left(\frac{c_L}{c_D}\right).$$

So, it is possible to maintain the kite at an equilibrium point with $\beta = \beta^\star$, $\phi = 0$, and with the angular velocities and angular accelerations equal to zero.

The equilibrium elevation varies approximately between 87° and 85° when the angle of attack varies between 0° and 12° degrees. For higher angles of attack, we obtain lower lift to drag ratios and, consequently, lower equilibrium elevations. For example, at 13.3^o we have a $\beta^* = 76^o$. This can be seen on Figure 4.12.

Chapter 5

A Trajectory Controller with Wind Gust Handling Capabilities

In this chapter we use the 3D simulation model of the kite dynamics to develop a path following algorithm and design a controller to follow the desired path. Then we address the problem of handling wind gusts, developing a method to prevent damage to the kite power system. We provide results obtained from our simulations and summarize the conclusions.

5.1 Trajectory Controller

In order to have a predictable behaviour, it is necessary to define a path for the kite to follow. Since our objective is to optimize the energy produced by the system, the path should be one where the kite moves mainly in crosswind during the production phase. Thus, we opted for a path like the one represented in Figure 5.1. In the retraction phase, we raise the kite's elevation angle to its equilibrium elevation, center it on the vertical plane $\phi = 0$, and pull the tether back. We develop a trajectory controller that allows the kite to follow the defined path.

5.1.1 Implementation

We define the path on the local (ϕ, β) coordinate system, contained in the spherical rectangle $\beta \in [30, 50]$, $\phi \in [-40, +40]$ degrees. The path consists of two straight lines and two semi circumferences, as can be seen in Figure 5.1. We create the four segments with a resolution we consider adequate, and concatenate them in the correct order, obtaining a 2D array of points with the (ϕ, β) coordinates of the complete trajectory.

Defining the trajectory on a (ϕ, β) coordinate system makes it independent of the tether length r. This way, the trajectory controller algorithm is separate from the tether reeling-out movement.

For the kite to follow the desired path we use a reference target approach to control its heading direction. Consider the position of the kite mass-point $\mathbf{p}(\phi, \beta)$. At each iteration, we determine the closest point to the desired path (A). Then, we define a point B in a forward direction along the path, at a distance L from A, which serves as a reference target. Finally, we determine an auxiliary

vector $\vec{L}_1$, which is the vector between p and B, and calculate the angle η between the kite velocity $\dot{p}$ and $\vec{L}_1$. The angle η is our reference to the kite desired heading direction adjustment. We act on the roll angle ψ using a proportional controller $\psi(t) = K\eta(t)$, in order to control the angle (η) towards zero. The L distance and the controller gain were adjusted empirically in order to obtain the best results. While a reference point B too close to A would lead to aggressive turns as the kite tries to follow the path, a reference point too far would make the kite skip some segments of the path. In both cases, the kite would eventually deviate too much from the desired path and get lost or even fall. The controller gain was also tuned to obtain a smooth kite trajectory. Controlling the kite trajectory through the heading directions, acting on the roll angle using a proportional controller, has been shown to be an adequate steering command [34].
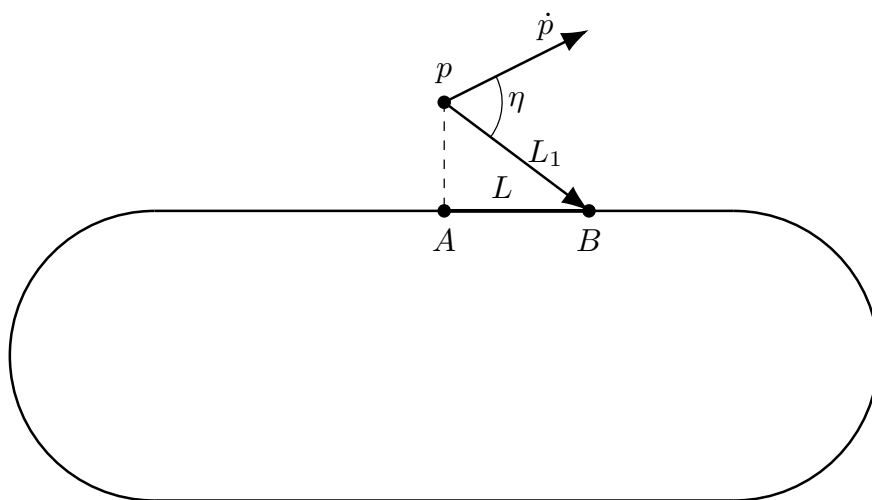

Figure 5.1: Trajectory Controller.

5.1.2 Simulations and Results

We start by simulating the system with a fixed tether length, and then we introduce the reel-out and reel-in movement to have a complete production cycle. In both simulations we first have a wind velocity of 10 m s^{-1}, then we increase the velocity to 30 m s^{-1} and finally we reduce it to 20 m s^{-1}.

Fixed Tether Length

Considering the case of a fixed tether length, we set the kite initial position to one not in the desired path. As can be seen in Figure 5.2, the kite follows the trajectory as intended with a small steady-state error. The state variables for this simulation can be seen on Figure 5.3. The control variables are shown in Figure 5.4. Since the kite is on a fixed tether length, a_t and α are constant, and we act only in the roll angle ψ. In Figure 5.5, the tether force in this simulation is shown.
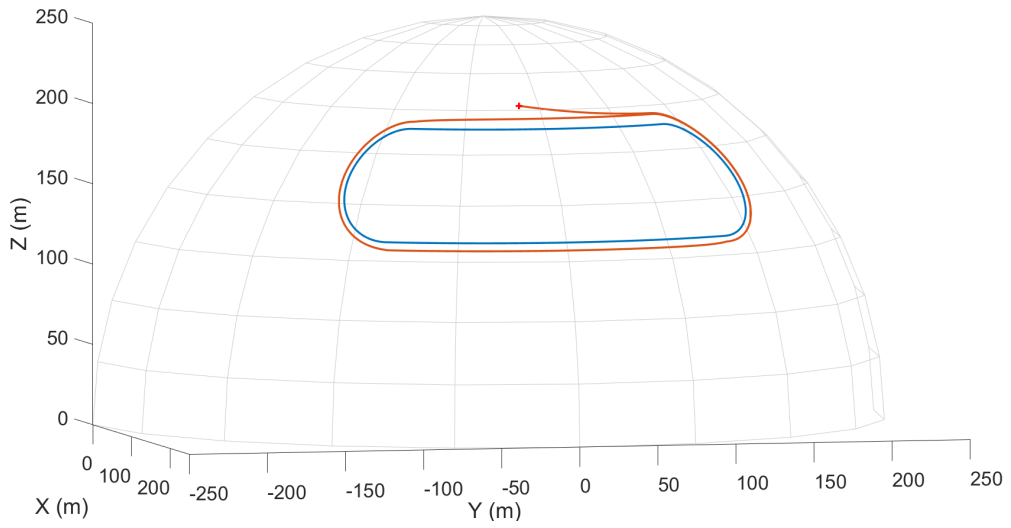
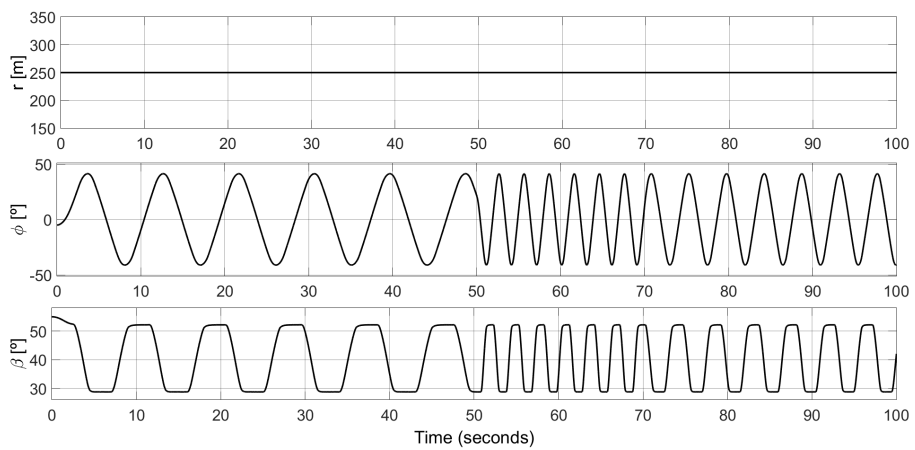Figure 5.2: Kite Trajectory with a fixed tether length.

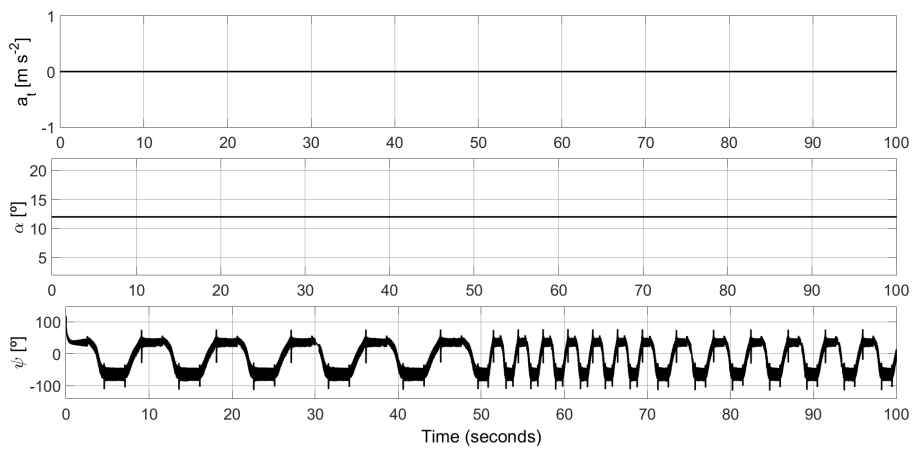Figure 5.3: State Variables (r, ϕ, β) of the Kite with a fixed tether length.

Figure 5.4: Control Variables (a_t, α, ψ) of the Kite with a fixed tether length.
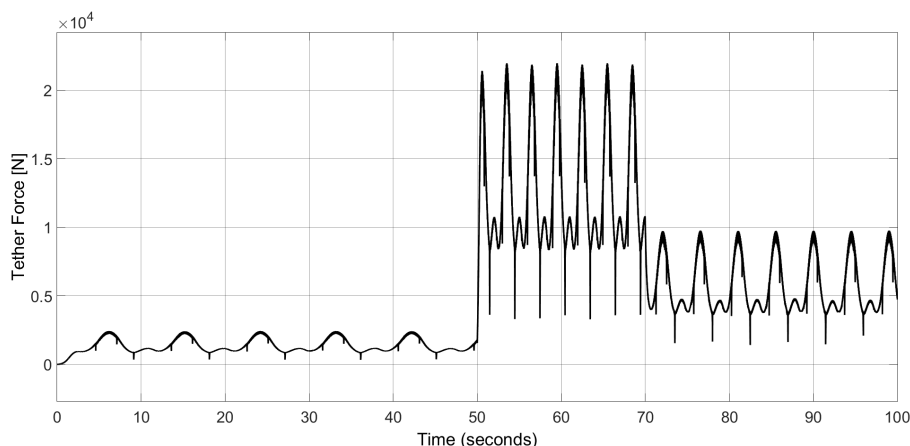
Figure 5.5: Tether Force.

Complete Production Cycle

We consider now the case of a complete production cycle, with the production phase in which the kite is following the defined trajectory, and the retraction phase where the kite is reeled-in. In Figure 5.6 the kite trajectory is shown. As we can see, the kite behaves as intended, following the desired trajectory during the production phase until it reaches the maximum tether length $r = r^{max}$. Then, it raises to its equilibrium elevation and centers in $\phi = 0$, and the cable is retracted until $r = r^{min}$. The state variables can be seen in Figure 5.7 and the control variables in Figure 5.8. We can see in Figure 5.9 the instant power output of the system and the energy production. As expected, the power output and consequently the energy production increases greatly with higher wind velocities.

5.2 Handling Wind Gust

Wind is highly inconsistent, and strong variations in its velocity, like a wind gust, can be dangerous for a system like this. As we could see from the previous simulations, the tether tension increases significantly with the wind velocity (see Figure 5.5), which can be above the tether physical limit. Thus, it is essential for a system like this to handle such variations. In this section we develop a safe strategy to handle strong wind velocities and prevent such high tether tensions.

5.2.1 Implementation

Even though the designed trajectory controller system is resilient enough to support certain strong wind velocities, as we could see from the previous simulations, in a real system the resultant tether tension force might be excessive for the tether, which can be dangerous for the system. To avoid this from happening, it is crucial to develop a method to handle wind gusts in a robust way.

So, for wind velocities that we consider above the safety limit, we develop a wind gust mode in which we elevate the kite towards the zenith, to an equilibrium elevation, and center it on the
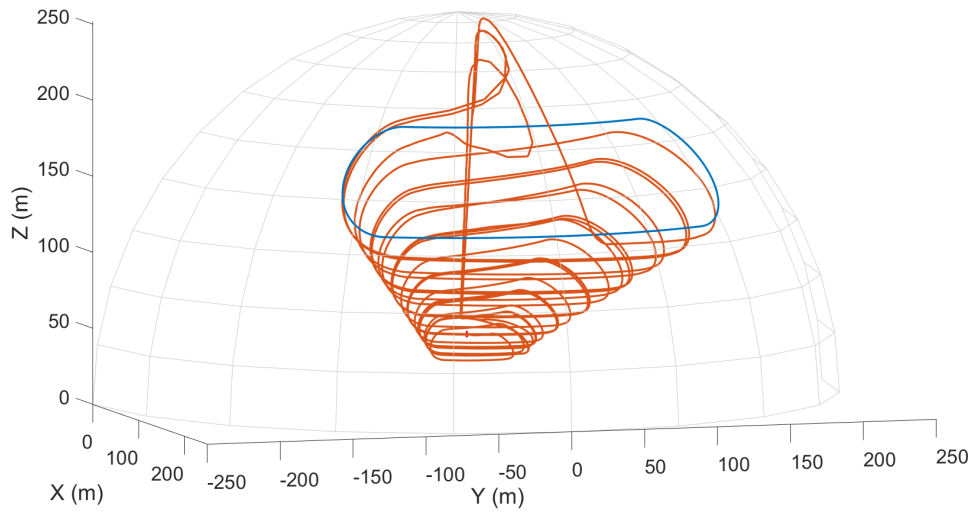
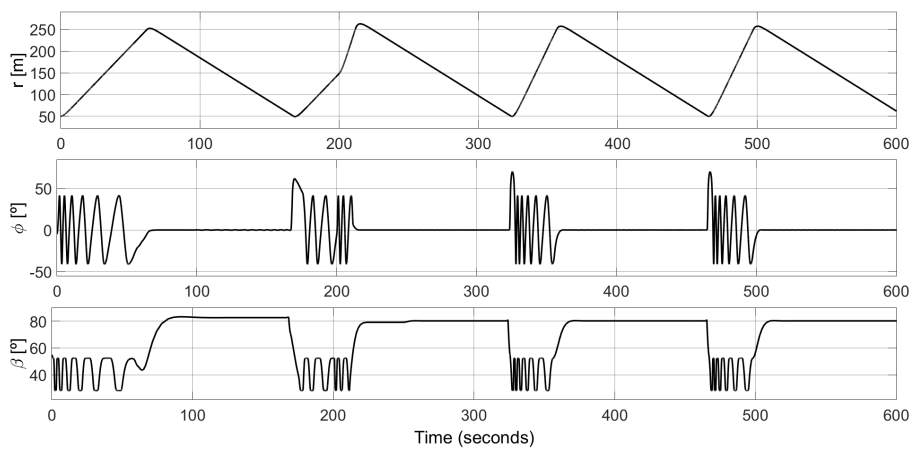Figure 5.6: Kite Trajectory in a complete production cycle.

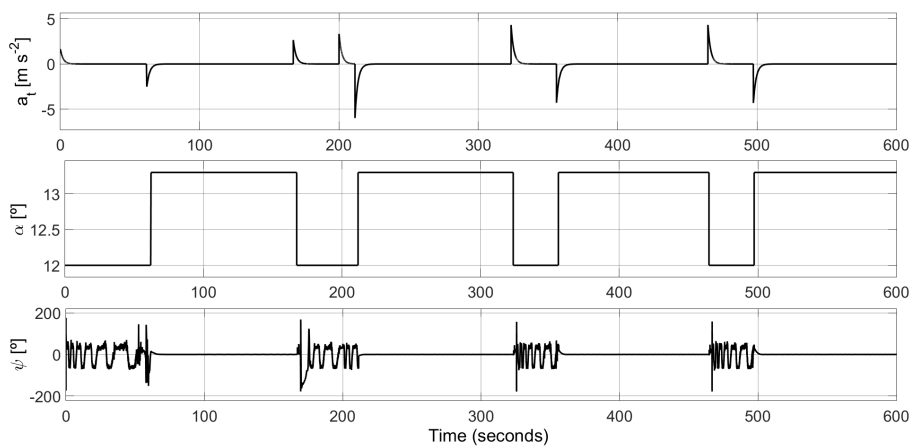Figure 5.7: State Variables (r, ϕ, β) of the Kite in a complete production cycle.

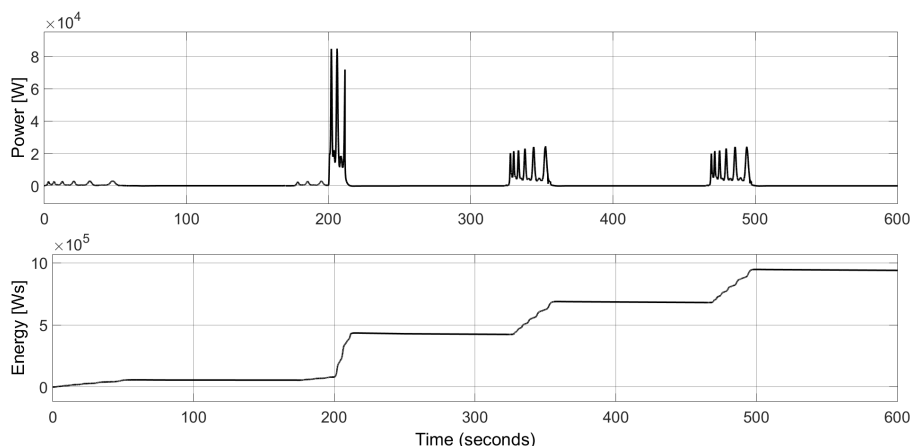Figure 5.8: Control Variables (a_t, α, ψ) of the Kite in a complete production cycle.

Figure 5.9: Power Output and Energy.

vertical plane ϕ=0. This is done by controlling the roll angle ψ. Also, we stop the tether reeling and set the angle of attack to a high value. With a high angle of attack we guarantee a low lift force, which minimizes the tether tension, but also a high drag force, stalling and decelerating the kite, avoiding uncontrollable movements. When the wind velocity returns to lower values, the system resumes to its normal behaviour.

5.2.2 Simulations and Results

Once again, we first simulate the system with a fixed tether length, and then with a complete production cycle. We use the same kite parameters and simulation times from the previous simulations. Wind velocity values are also the same, that is, we start with 10 m s^{-1}, increase it to 30 m s^{-1} and finally reduce it to 20 m s^{-1}. We consider that the wind gust mode should activate for wind velocities above 25 m s^{-1}.

Fixed Tether Length

As before, we start by simulating the system with a fixed tether length, and see how the kite reacts to a wind gust. We can see in Figure 5.10 that the kite follows the desired path, and when wind velocity reaches the defined threshold, the gust mode is activated. The kite is then centered in $\phi = 0$ and elevated to an equilibrium elevation. As the gust stops, this is, wind velocity returns to lower values, the kite descends and returns to the desired path. The state and control variables can be seen in Figures 5.11 and 5.12, respectively. We can see that during the wind gust mode, $\psi = 0$ and α is set to a value which produces a lower lift force but a higher drag, allowing for the kite to stay in the intended position. In Figure 5.13, we can see the tether force in this simulation. Comparing with Figure 5.5, for the same wind velocity values, we can significantly reduce the the tether tension with this strategy, making it an effective way to handle strong winds.
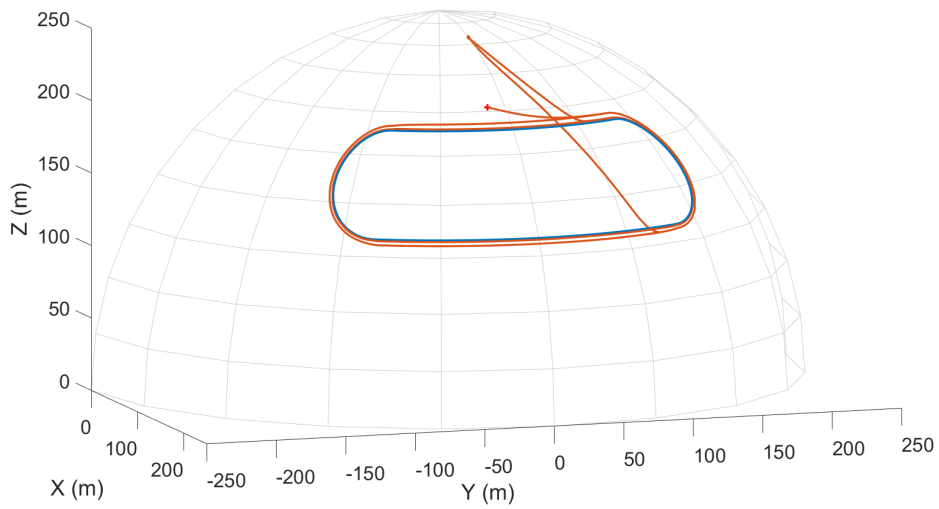
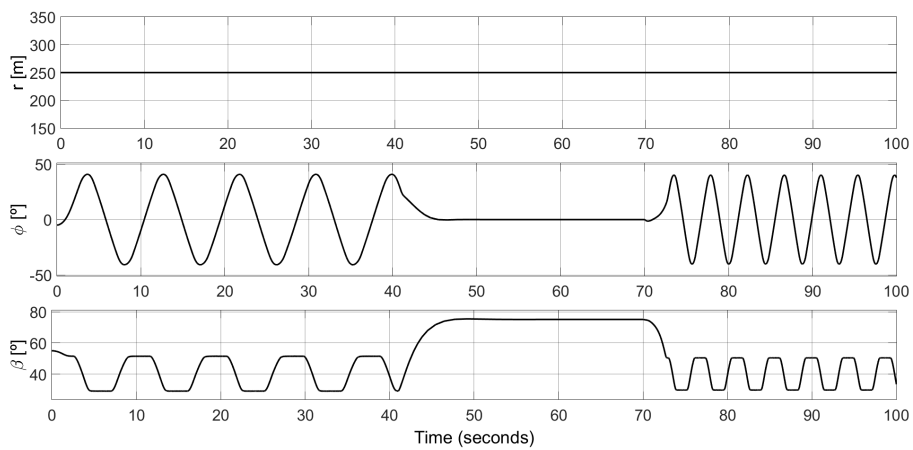Figure 5.10: Kite Trajectory with wind gust mode.

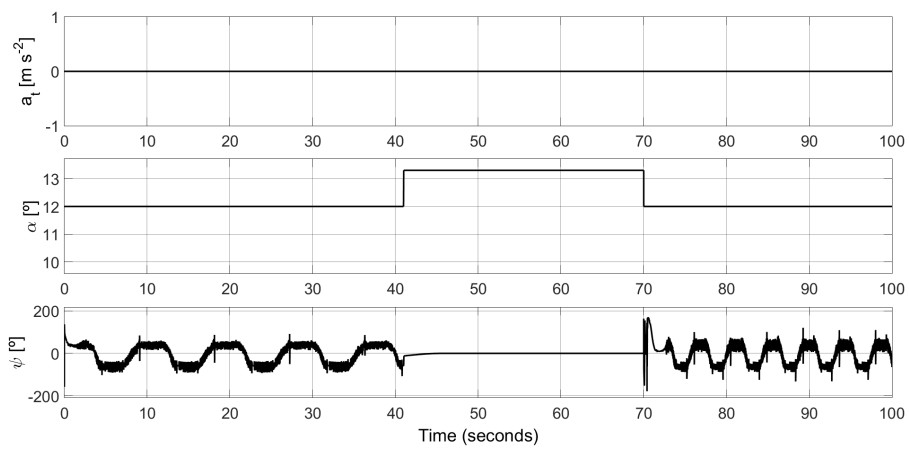Figure 5.11: State Variables (r, ϕ, β) with a fixed tether length and wind gust mode.

Figure 5.12: Control Variables (a_t, α, ψ) with a fixed tether length and wind gust mode.
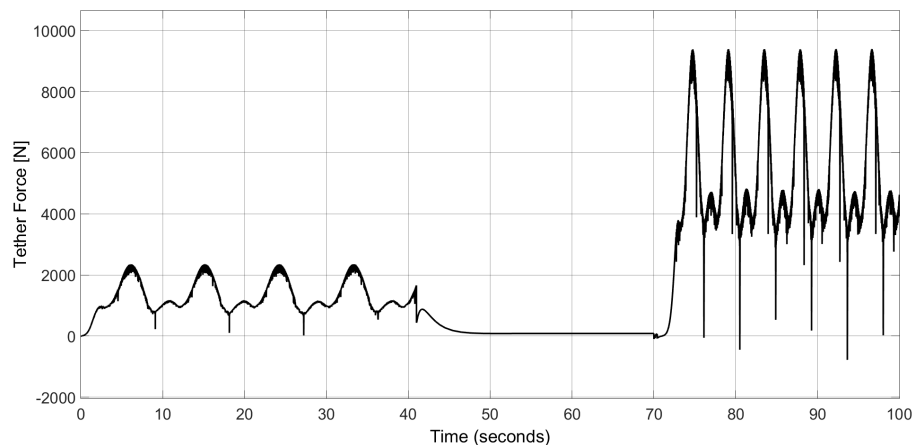
Figure 5.13: Tether Force.

Complete Production Cycle

Now we see an example of a complete production cycle, with the reel-out and reel-in of the tether. As we can see on Figure 5.14, as the kite rises and a wind gust occurs, the reeling out of the tether is stopped and the kite is elevated to an equilibrium point, returning to the trajectory as wind velocities return to lower values.

On Figure 5.15 we can see the state variables (r, ϕ, β). We clearly see the wind gust occurring between $[200, 250]s$, as r stays constant, ϕ goes to zero and the elevation angle β rises. On Figure 5.16 we can see the control variables, and as supposed, during the wind gust we have a high angle of attack (α) and ψ is zero since the kite is centered on $\phi = 0$. Finally, on Figure 5.17, we can see energy is produced during the reel-out phase, and a slight amount is spent during the reel-in phase. During the gust mode, energy is neither produced or spent.

5.3   Discussion

In this chapter a trajectory controller to follow a pre-defined path was developed. Even though the developed controller can keep the kite following the path even with strong wind velocities, the resultant tether tension might be too much for the tether to handle. So, we define a wind velocity threshold for which we assume that it is not safe to operate the system in a regular way. For wind velocities above the threshold, we develop a safety wind gust mode in which we elevate the kite to an equilibrium point with an angle of attack that minimizes the tether tension.

Comparing Figures 5.5 and 5.13, we can see that, for the same wind velocity values, this mode drastically reduces the tether tension. We consider the results to be very satisfying and this mode to be an effective way to handle wind gusts.
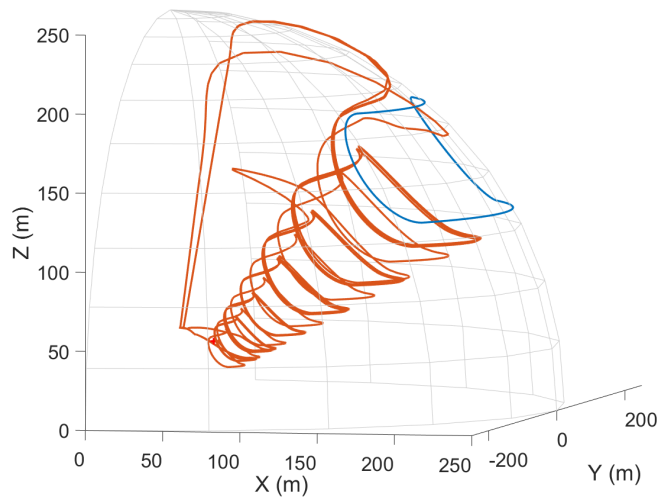
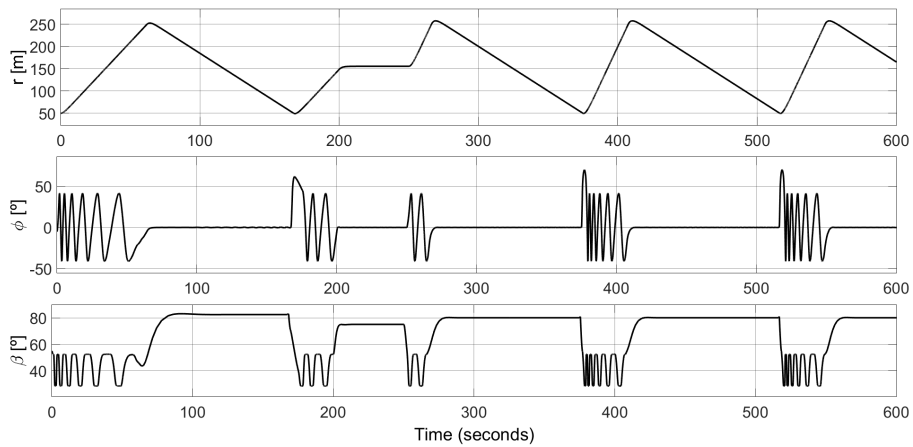Figure 5.14: Kite Trajectory in a complete production cycle with gust mode.

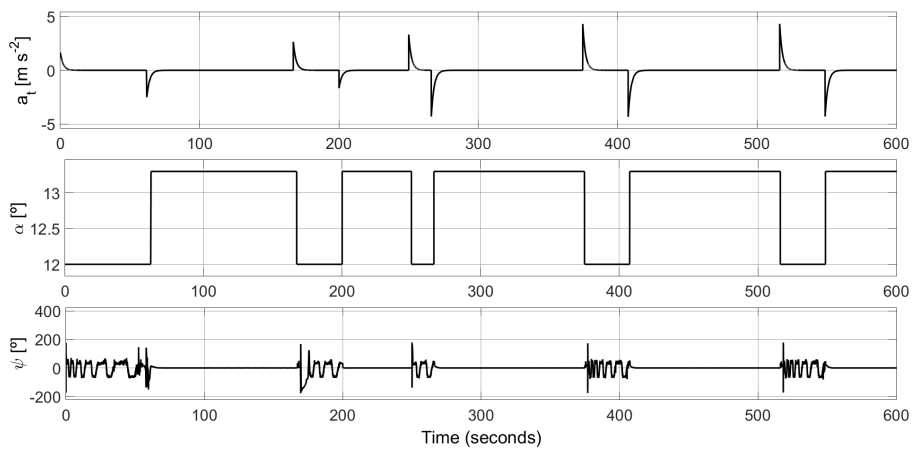Figure 5.15: State Variables (r, ϕ, β) of the Kite in a complete production cycle with gust mode.

Figure 5.16: Control Variables (a_t, α, ψ) of the Kite in a complete production cycle with gust mode.
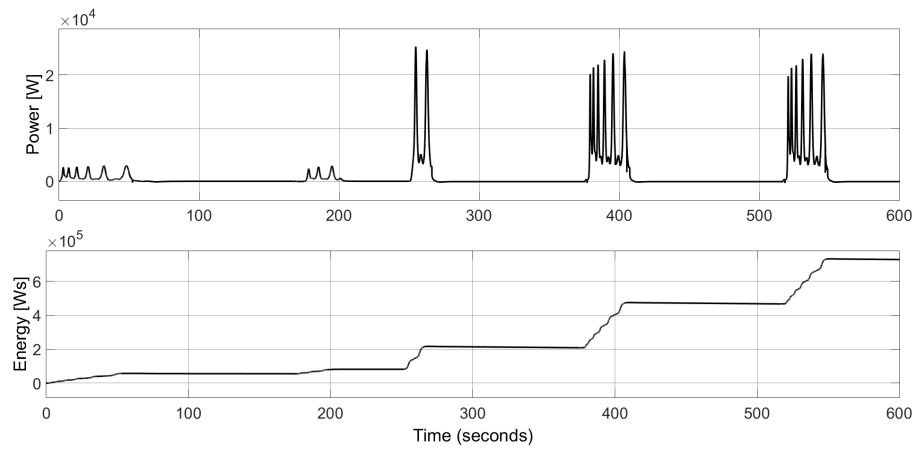
Figure 5.17: Power Output and Energy.

Chapter 6

Path Following and Heading Angle Control of a KPS

In this chapter we develop a controller based on a nonlinear guidance logic as in [8]. We explain the basis behind this algorithm and find a mathematical relation to apply it to the KPS. Then, we simulate the system with different trajectories and discuss the results. Finally, we provide a Lyapunov stability analysis.

6.1 Nonlinear Guidance Logic

The Nonlinear Guidance Logic for Trajectory Tracking [8] utilizes the inertial speed of the vehicle to determine a lateral acceleration command. This logic is specially good for curved trajectories.

The algorithm consists of two steps. First, we select the reference point on the desired path for the vehicle to follow. While in [8] the reference point is always at a fixed L_1 distance, in our implementation we utilize a similar strategy as in Chapter 5. Thus, we find the closest point to the kite in the desired path, and then determine a reference point at a distance L from it (see Figure 5.1). With our approach, length L_1 is variable, however, the advantage of this method is that we can always find a reference point even if the kite moves too far from the path. With a fixed distance L_1, if the kite moves to a distance d bigger than L_1 it would be necessary to develop another method for it to return to the desired path.

The second step of this algorithm is to calculate the lateral acceleration command. As in [8], this is determined by

$$a_{s_{cmd}} = 2\frac{V^2}{L_1}sin(\eta).$$ (6.1)

The basis of this algorithm is that, at each iteration, a circular path tangent to the vehicle velocity vector can be defined by the reference point and the vehicle position (see Figure 6.1).

The lateral acceleration command $a_{s_{cmd}}$, determined by equation 6.1, is equal to the centripetal acceleration necessary to follow the circular segment. We can see by Figure 6.2 that $L_1 = 2Rsin\eta$.
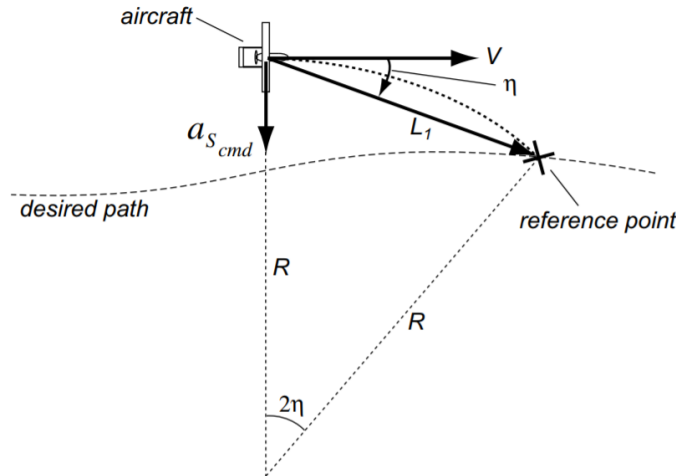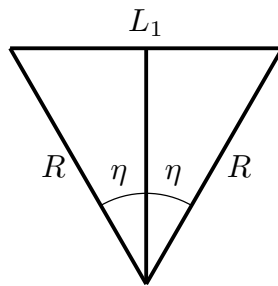
Figure 6.1: Diagram for Guidance Logic [8].

Figure 6.2: L_1 length.

Thus, the centripetal acceleration is determined by

$$centripetal\ acceleration = \frac{V^2}{R} \implies 2\frac{V^2}{L1}\sin\eta = a_{s_{cmd}}. \tag{6.2}$$

In this algorithm, the direction of the acceleration command depends on the sign of the angle between the vehicle velocity V and L_1, so the velocity vector direction tends to align with L_1. This property leads to a smooth convergence to the desired path, as can be seen in Figure 6.3. When the vehicle is far away from the desired path, the direction of L_1 makes a large angle with the path, so the velocity vector approaches the path at a large angle. When the vehicle is close to the path, L_1 makes a small angle with the path, thus the velocity vector approaches the path at a small angle.

6.2 Heading Angle Control

In order to apply the guidance logic presented above, a relation between the roll angle ψ and the centripetal acceleration a_c has to be found. The controller calculates the roll angle ψ necessary to fly a curve with a certain radius at a constant altitude [35].
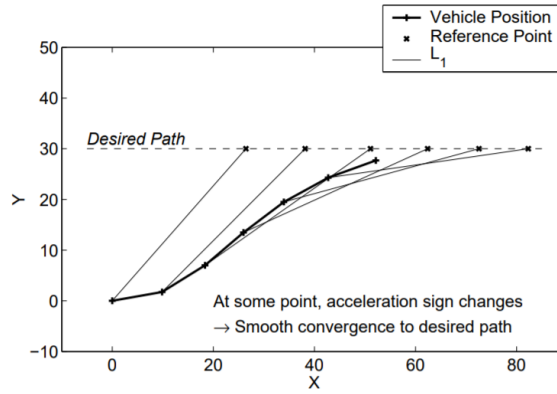
Figure 6.3: Iterations of vehicle approaching the trajectory [8].

Consider the case represented in Figure 6.4, in which the kite is at a distance d from the path. We assume the tether on a fixed length r, and the trajectory to be defined in (ϕ, β), approximately in the plane τ tangent to the sphere with radius r.
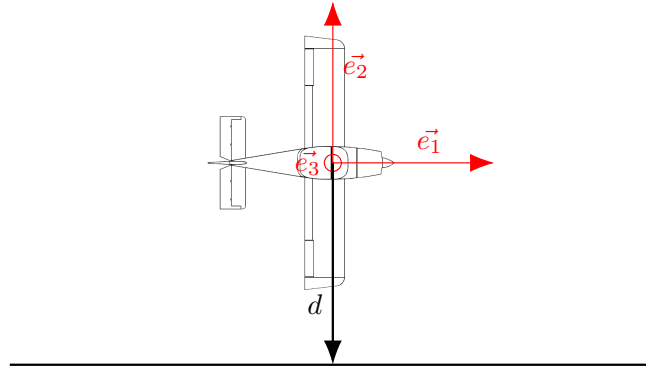

Figure 6.4: Heading Angle Control Example.

The lift force acting on the kite is given by

$$\vec{F}^{\text{lift}}(\alpha) = \frac{1}{2}\rho A c_{\text{L}}(\alpha)\|\mathbf{v}_a\|^2\vec{\mathbf{e}}_3. \tag{6.3}$$

Considering the case where the roll angle $\psi = 0$, the $\vec{F}^{\text{lift}}$ vector has only a vertical component (see Figure 6.5).

We assume that $\vec{d}$ is in the tangent plane τ. So,

$$\frac{\vec{d}}{\|d\|} = -\vec{\mathbf{e}}_2 \ if \ \psi = 0. \tag{6.4}$$

That is, if $\psi = 0$, then $\vec{d}$ is aligned with the kite's right wing.

Consider now the case for a roll angle $\psi > 0$. The $\vec{F}^{\text{lift}}$ vector is tilted by the same angle, and can be divided into a vertical and horizontal component (see Figure 6.6).
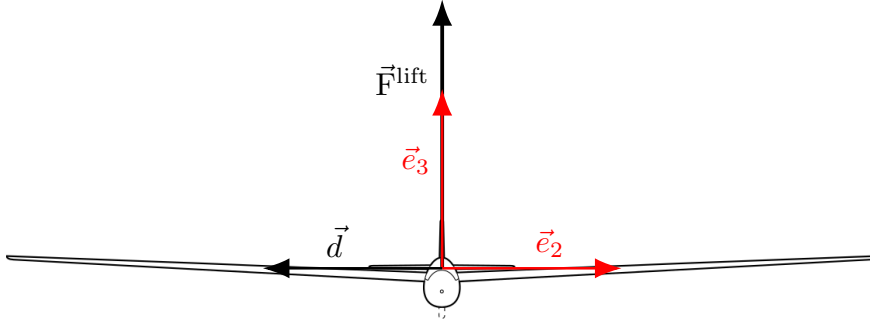
Figure 6.5: Kite Front-view with $\psi = 0$.
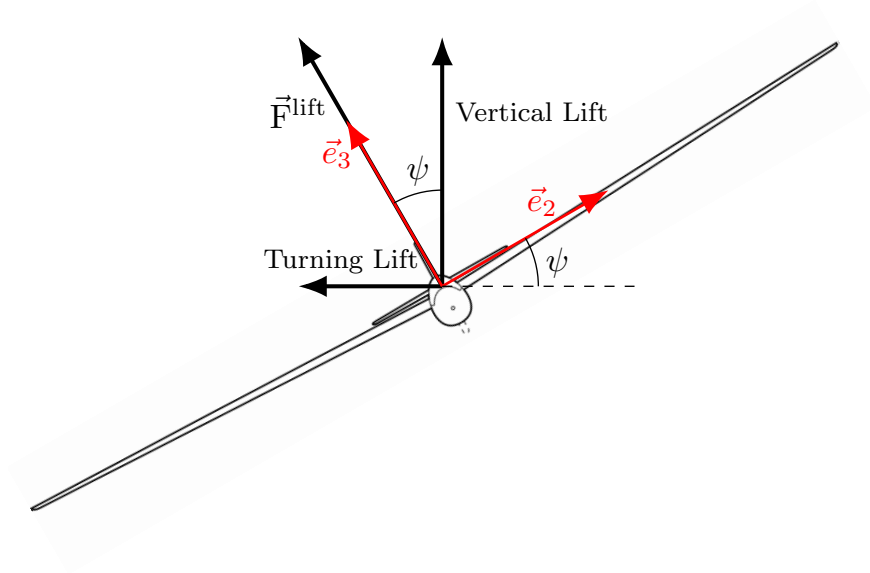
Figure 6.6: Aircraft in a turn.

Thus, the horizontal lift component acts as a centripetal force. The centripetal acceleration of the kite is then given by

$$a_c = \frac{\vec{F}^{\text{lift}}\sin(\psi)}{m}. \tag{6.5}$$

Matching expressions (6.1) and (6.5), we have

$$\frac{\vec{F}^{\text{lift}}\sin(\psi)}{m} = 2\frac{V^2}{L_1}sin(\eta) \tag{6.6}$$

and solving it in order to ψ, we obtain

$$\psi = \arcsin\left(2m\frac{V^2 sin(\eta)}{\vec{F}^{\text{lift}}L_1}\right). \tag{6.7}$$

ψ is a function of arcsin, which is only real in the interval $[-1;1]$. Therefore, the values outside that interval were saturated in those limits. This way, we obtain values of $\psi \in [-\frac{\pi}{2}; \frac{\pi}{2}]$.

6.3 Simulation Results

6.3.1 Elliptical Path

We apply this new control algorithm to an elliptical path with a fixed tether length. The simulation parameters are the ones in Table 4.2. As we can see in Figure 6.7, the kite follows the intended path quite well. In comparison with the trajectory controller implemented in 5, since this algorithm is based on the centripetal acceleration, we had to convert the defined path from the spherical coordinate system (r, ϕ, β) to the global cartesian coordinate system (x, y, z). This happens because our control command is calculated as a function of the centripetal acceleration, which is in $\mathrm{m\,s^{-2}}$. Thus, we have to consider the global coordinate system to ensure our units in meters. The state variables for this simulation are represented in Figure 6.8 and the control variables in Figure 6.9.
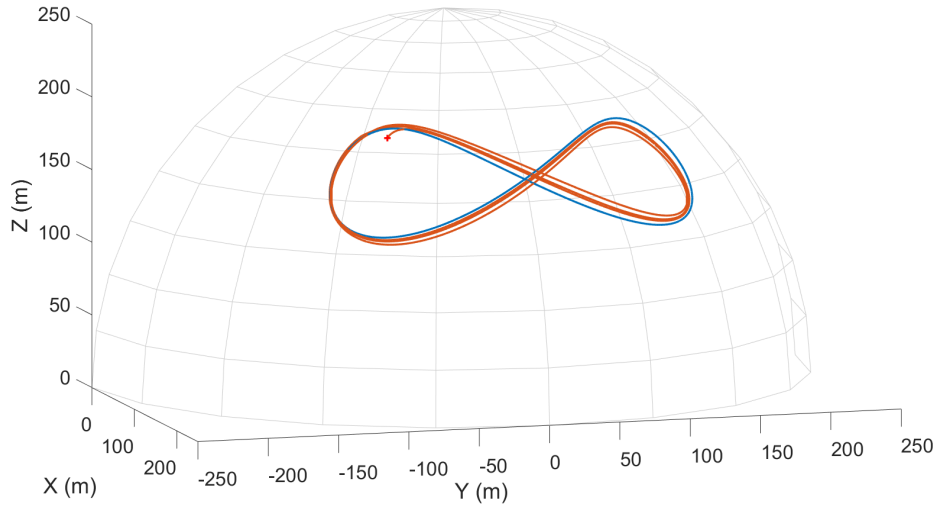

Figure 6.7: Elliptical Trajectory.

6.3.2 Eight-shape Path

We applied the same algorithm but to an eight-shape path. The trajectory is a Lissajous Curve, with a relation $a/b = 2$, this is, the frequency in β is double the frequency in ϕ:

$$\begin{cases} \phi = \phi_0 + \Delta\phi \cos(t), \\ \beta = \beta_0 + \Delta\beta \sin(2t). \end{cases} \tag{6.8}$$

This trajectory has the advantage of having both curves in the same direction, i.e. both curves are either in ascending direction or in descending direction. In an elliptical path, one curve is
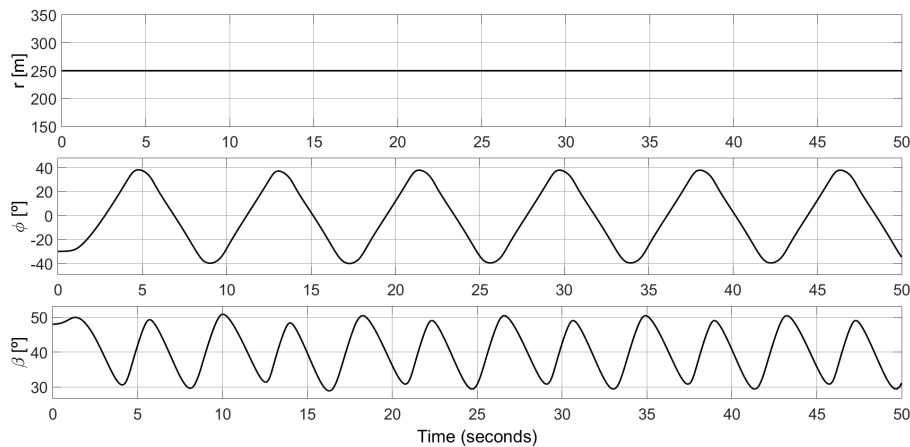
Figure 6.8: State variables (r, ϕ, β) for Elliptical trajectory with constant tether length.
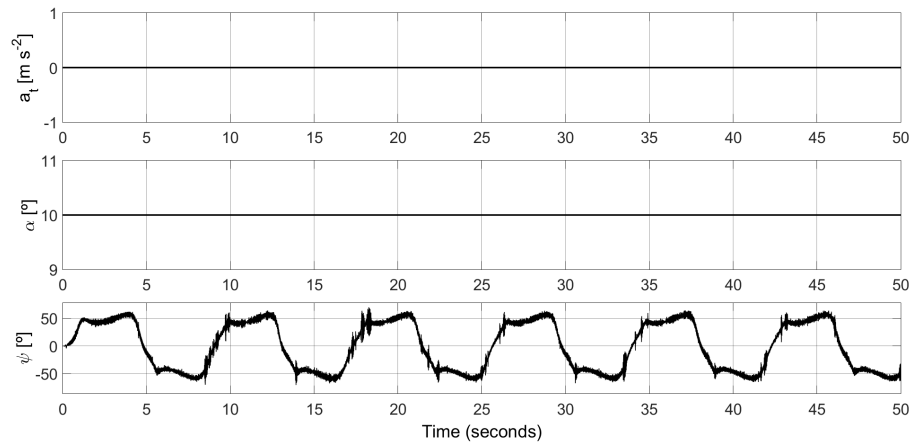

Figure 6.9: Control Variables (a_t, α, ψ) for Elliptical trajectory with constant tether length.

in ascending direction and the other in descending direction. In a real system, the eight-shape trajectory is also used to prevent line entanglement.

Since the path has an intersection in the middle, the algorithm to find the closest point in the path had to be adapted. Thus, instead of searching for the closest point in the whole path, we save the index of the last reference point. Then, since the path is a sorted array with the path coordinates, we search for the closest point only in a limited range starting from the saved reference point. This way, the algorithm is optimized and the reference point is correctly determined at all times.

In Figure 6.10 we can see the kite following the trajectory with a fixed tether length. The path is defined in $\phi \in [-40, 40]$ and $\beta \in [30, 50]$. The state variables for this simulation can be seen in Figure 6.11. In Figure 6.12 we can see the control variables.
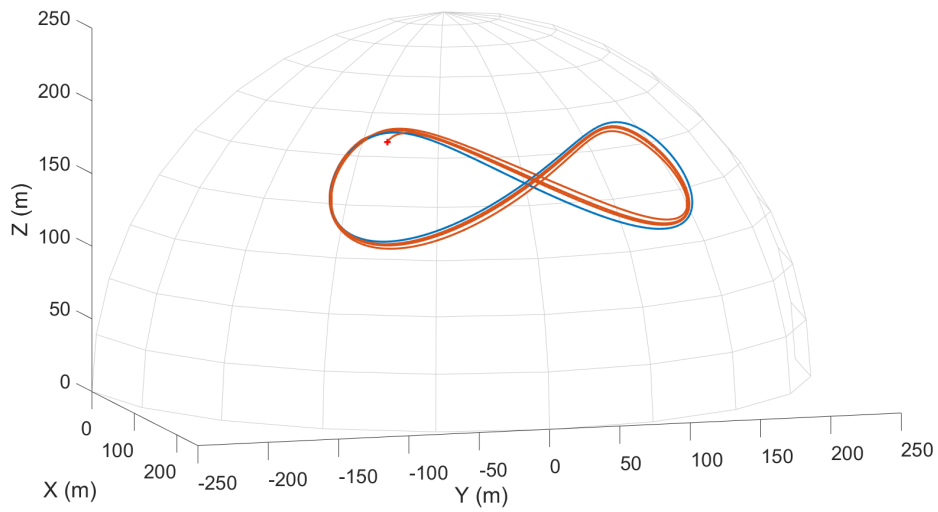
Figure 6.10: Eight-shape Kite Trajectory with fixed tether length.
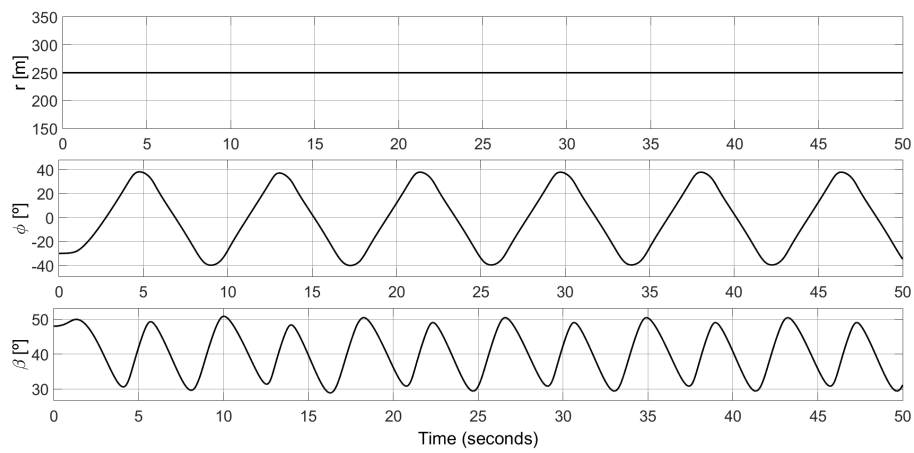
Figure 6.11: State variables (r, ϕ, β) for Eight-shape trajectory with fixed tether length.
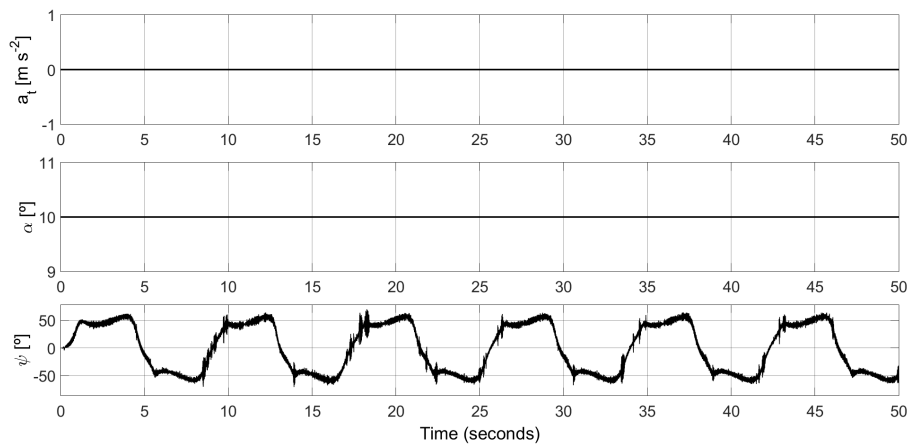
Figure 6.12: Control variables (a_t, α, ψ) for Eight-shape trajectory with fixed tether length.

In Figure 6.13 we simulate a complete production cycle for the eight-shape path. The state variables are represented in Figure 6.14. In Figure 6.15 we can see the control variables and in Figure 6.16 the power output and energy production of the system.

Figure 6.13: Complete production cycle with an eight-shape trajectory.
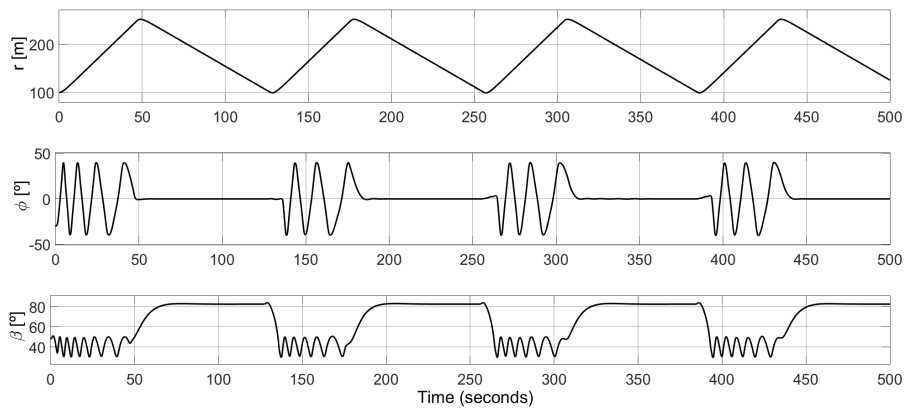
Figure 6.14: State variables (r, ϕ, β) for full production cycle on eight-shape trajectory.
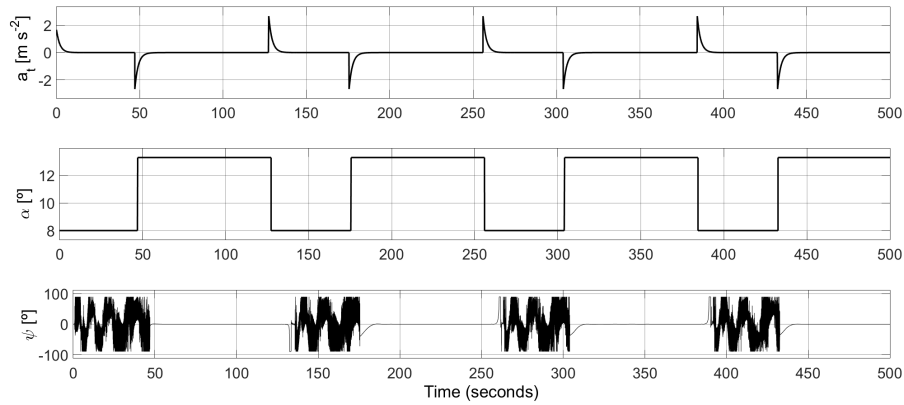
Figure 6.15: Control variables (a_t, α, ψ) for full production cycle on eight-shape trajectory.
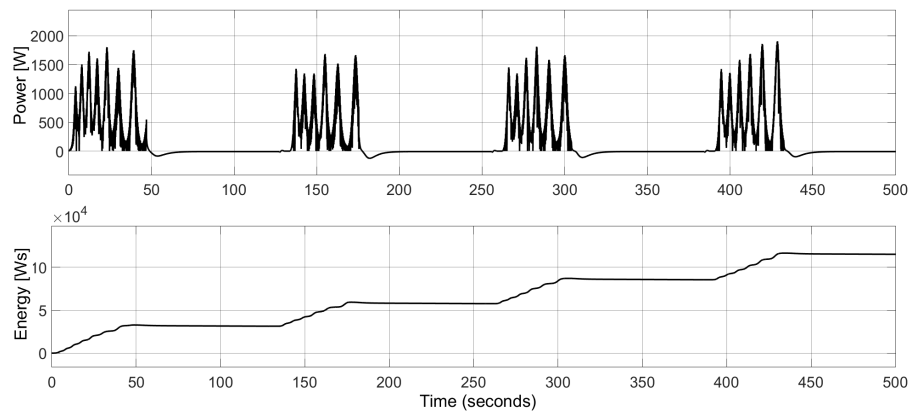
Figure 6.16: Power and Energy.

6.4 Discussion

The simulation results show that the the guidance logic algorithm was successfully implemented. We start by defining an elliptical path, similar to what was done in 5, and t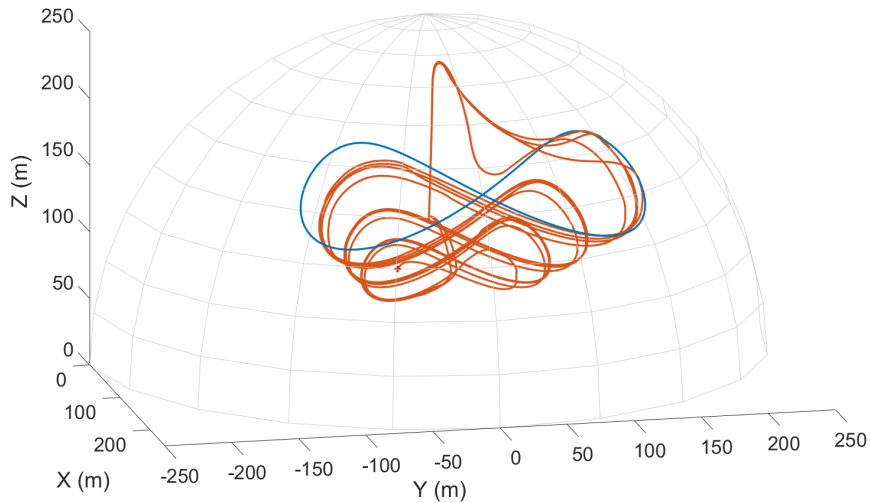hen an eight-shaped path. In both cases, the kite follows the desired trajectories. The advantage of the eight-shaped path is that both curves are in the same direction, which in our simulations are in ascending direction. In Figure 6.13 we can see a complete production cycle with an eight-shaped path. With $r_{min} = 100$ and $r_{max} = 250$, and a reel-out speed of around $1/3 v_w$, we attain an average power of 240W. One reason for the low efficiency of the system is due to the recovery phase, which takes too long and needs to be optimized. We can achieve instant power peaks of up to 1800W (see Figure 6.16).

6.5   Lyapunov Stability Analysis

In this section we provide a Lyapunov stability analysis for the case when the kite is following a straight line path. This analysis is adapted from [8] to the case when L is fixed and L_1 is varying.
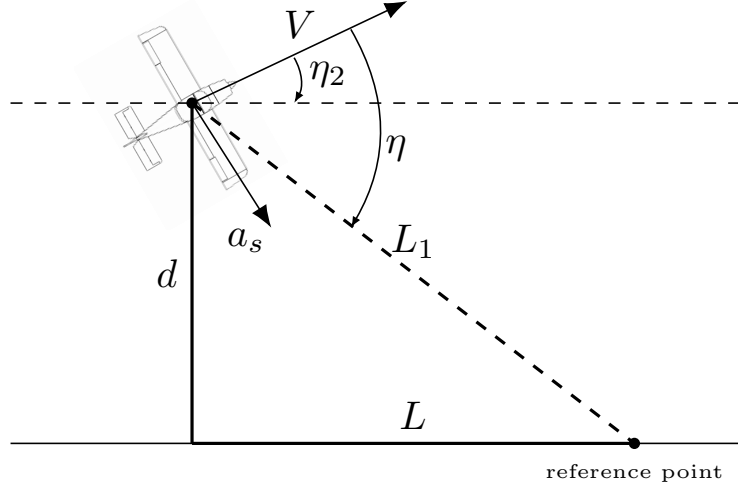
Figure 6.17: Model for Lyapunov Analysis for Straight Line Following Case.

We consider that the deviation from the path can be described by the transversal distance d and the angle η_2 (see Figure 6.17).

$$\begin{cases} \dot{d} = V \sin \eta_2 \\ \dot{\eta}_2 = -\dfrac{a_s}{V} \end{cases} \tag{6.9}$$

with a_s being the guidance logic determined by

$$a_s = 2\frac{V^2}{L_1}sin(\eta). \tag{6.10}$$

Consider the unique existence of the reference point. We assume that

$$\frac{-\pi}{2} < \eta < \frac{\pi}{2}. \tag{6.11}$$

We aim to show that the system stabilizes at $(d, \eta_2) = (0,0)$. This is achieved by showing that

$$\mathscr{L} = \frac{1}{2}(V \sin \eta_2)^2 + \int_0^d \frac{2\,V^2}{\sqrt{L^2 + y^2}} \sin(\eta - \eta_2) dy \tag{6.12}$$

is a Lyapunov function. From Figure 6.17, we can write

$$\sin(\eta - \eta_2) = \frac{d}{L_1} = \frac{d}{\sqrt{L^2 + d^2}}. \tag{6.13}$$

Then, Eq. (6.12) becomes

$$\mathscr{L} = \frac{1}{2}(V \sin \eta_2)^2 + \int_0^d \frac{2\,V^2}{\sqrt{L^2 + y^2}} \frac{y}{\sqrt{L^2 + y^2}} dy$$

$$= \frac{1}{2}(V \sin \eta_2)^2 + V^2 \int_0^d \frac{2\,y}{L^2 + y^2} dy$$

$$= \frac{1}{2}V^2 \sin^2 \eta_2 + V^2 \ln(L^2 + y^2)\Big|_0^d$$

$$= \frac{1}{2}V^2 \sin^2 \eta_2 + V^2 \left(\ln(L^2 + d^2) - \ln(L^2)\right), \tag{6.14}$$

which is a positive definite function. Next, the time derivative of Eq. (6.14) is

$$\dot{\mathscr{L}} = \frac{1}{2}\,V^2\,2 \sin \eta_2 \cos \eta_2 \dot{\eta}_2 + V^2 \frac{2d}{L^2 + d^2} d$$

$$= V^2 \sin \eta_2 \cos \eta_2 \left(-\frac{a_s}{V}\right) + V^2 \frac{2d}{L^2 + d^2} V \sin \eta_2$$

$$= -\frac{2V^3}{L_1} \sin \eta_2 \cos \eta_2 \sin \eta + 2V^3 \frac{d}{L_1^2} \sin \eta_2$$

$$= -\frac{2V^3}{L_1} \sin \eta_2 \left(\cos \eta_2 \sin \eta - \frac{d}{L_1}\right). \tag{6.15}$$

Using Eq. (6.13), we can write Eq. (6.15) as

$$\dot{\mathscr{L}} = -\frac{2V^3}{L_1} \sin \eta_2 \left(\cos \eta_2 \sin \eta - \sin(\eta - \eta_2)\right).$$

Finally, using

$$\sin(\eta - \eta_2) = \sin \eta \cos \eta_2 - \cos \eta \sin \eta_2$$

$\dot{\mathscr{L}}$ is reduced to

$$\dot{\mathscr{L}} = -\frac{2V^3}{L_1} \sin^2 \eta_2 \cos \eta$$

$$= -\frac{2V^3}{\sqrt{L^2 + d^2}} \sin^2 \eta_2 \cos \eta, \tag{6.16}$$

which is a negative semi-definite function since $|\eta| < \pi/2$, guaranteeing stability. Then, applying the invariant set theorem A.3, the set defined by $\dot{\mathscr{L}} = 0$ contains no trajectory other than $(d, \eta_2) = (0,0)$. Therefore, $(d, \eta_2) = (0,0)$ is asymptotically stable for $|\eta| < \pi/2$.

Also, when $d \to \infty \Rightarrow \mathscr{L} \to \infty$. Thus, the system domain of attraction is

$$\left\{(d, \eta_2) \in \mathbb{R} \times [-\pi, \pi] : -\frac{\pi}{2} < \eta_2 < \frac{\pi}{2}\right\}. \tag{6.17}$$

Chapter 7

Conclusions and Future Work

7.1 Conclusions

In this dissertation we address the problem of AWES. High wind energy has a huge potential as wind velocities are considerably stronger at high altitudes, and many different ideas to extract that energy have been proposed by companies. It is, however, with the fast development over the last few years that these systems are approaching economic competitiveness.

We introduce the KPS model, and did some simulations with simplified 2D versions of it. While the Underwater Kite problem was shown to be an effective way to produce electrical energy, we concluded that the 2D AWES strategy is not efficient to be pursued.

Then, using the complete 3D dynamic simulation model, we develop a method to control the kite in order to follow a pre-defined path, based on a heading proportional controller. The chosen path is an elliptical rectangle defined only in (ϕ, β) and is independent of the tether length and reel-out speed. The kite is steered by acting on the roll angle (ψ). Even though the controller is robust even for high wind velocities, a safety mode is developed to avoid excessive tension on the tether. For wind speeds above a certain threshold, the kite is driven towards the zenith. The reeling movement is stopped and the angle of attack is set to a value that decreases the tether tension. The developed strategy was shown to be an effective way to handle wind gusts.

Finally, we propose and test an alternative trajectory controller based on a state-of-the-art nonlinear guidance logic developed at MIT [8]. The controller uses the kite inertial speed to determine a lateral acceleration command, which is equal to the centripetal acceleration necessary to follow a circular segment defined at each iteration. The trajectory controller was successfully adapted for the KPS problem, as the kite is capable of following the desired path, either it is an elliptical path or an eight-shaped path. Also, we provide a Lyapunov stability analysis for the case the kite is following a straight line desired path. The system is shown to be asymptotically stable for $|\eta| < \pi/2$.

7.2 Future Work

The UP Wind project is just now starting so there is a lot of work to do. In the specific case of this dissertation, even though the main goals were achieved, there is still room for improvements. The guidance logic algorithm was successfully implemented, although it still needs a slight tuning before applying it to a real system.

The angle of attack control also needs to be developed, as in this dissertation we assume we can instantly set it to a desired value, which is not possible in a real system. In the future, we should have a controller for the roll angle ψ and another for the angle of attack α that work together as the kite follows the path. Also, we set the angle of attack to a high value to induce a high drag force in the kite while maintaining a low lift force. This is useful as it allows us to stall the kite, and retract it back without losing control of it. In a real system this could be achieved using a wing flap system for example, inducing drag to the kite while maintaining a small angle of attack.

The recovery phase is another aspect that needs improvement. Ideally, this phase should be shorter than production phase for the system to be effective. Thus, that is something that should to be optimized as we could not achieve fast reel-in speeds in our simulations.

The take-off and landing maneuvers is something we did not address in this dissertation and are a crucial part on these systems operation. Therefore, strategies should be considered for a safe take-off and landing of the kite power system.

An ambitious project like this one involves many different topics and there will be always improvements to be made. This technology is still far from being completely dominated, and there is a window of opportunity in the development of new controllers and improvement of the existing methodologies. The final objective is to build real prototypes and test them, first as a single kite system, and then as a multiple kite system.

Appendix A

Lyapunov Stability Theory

This appendix is an introduction to Lyapunov stability theory and addresses some important definitions. It is essentially based on Chapter 3, "Fundamentals of Lyapunov Stability Theory", of the book Applied Nonlinear Control [36], by Slotine and Li.

A.1 Concepts of Stability

We start by introducing the definition of equilibrium state.

Definition A.1 ([36]) *A state x^* is an equilibrium state (or equilibrium point) of the system if once $x(t)$ is equal to x^*, it remains equal to x^* for all future time.*

Now we can introduce the basic concepts of stability and instability.

Definition A.2 ([36]) *The equilibrium state $x = 0$ is said to be <u>stable</u> if, for any $R > 0$, there exists $r > 0$, such that if $||x(0)|| < r$, then $||x(t)|| < R$ for all $t \geq 0$. Otherwise, the equilibrium point is <u>unstable</u>.*

Mathematically, this definition can be written

$$\forall R > 0, \exists r > 0, ||x(0)|| < r \Rightarrow \forall t \geq 0, ||x(t)|| < R \tag{A.1}$$

This means that, if the origin is an equilibrium state, a trajectory starting sufficiently close to the origin can be kept close to it.

For some applications though, the concept of stability presented above is not enough. If we want a trajectory that, not only stays close to the origin, but actually converges to it, we need to address a new concept of stability, called asymptotic stability.

Definition A.3 ([36]) *An equilibrium point $\boldsymbol{0}$ is <u>asymptotically stable</u> if it is stable, and if in addition there exists some $r > 0$ such that $||x(0)|| < r$ implies that $x(t) \rightarrow 0$ as $t \rightarrow \infty$.*

The set of points such that trajectories initiated on them converge to the origin is called domain of attraction. An equilibrium point which is Lyapunov stable but not asymptotically stable is called *marginally stable*.

In other words, the previous definitions mean that for a trajectory starting inside a ball with radius S_r ($x(0) \in S_r$), if the trajectory x(t) stays inside of a ball with radius S_R ($x(t) \in S_R \forall t \geq 0$) we can consider the origin is stable. Furthermore, if the trajectory actually converges to the origin, the equilibrium point 0 is called asymptotically stable and the ball S_r is the domain of attraction. This can be seen on figure A.1.
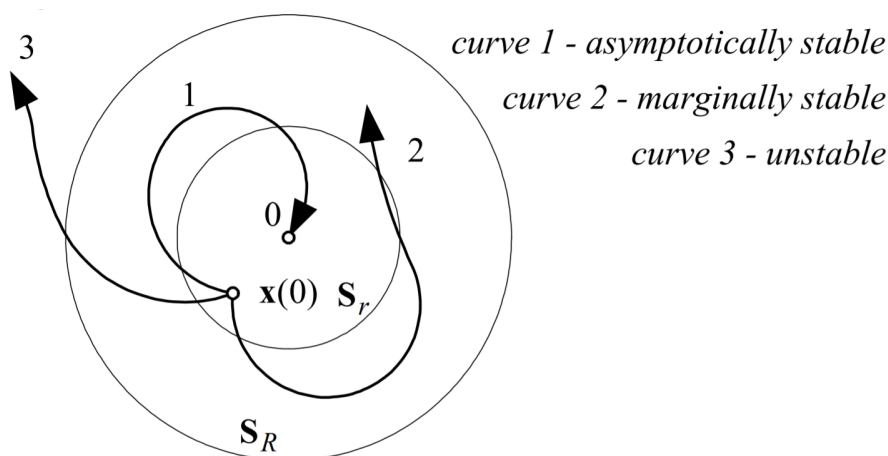

Figure A.1: Concepts of Stability [36]

Sometimes it is also interesting to estimate how fast the system trajectory approaches 0, and for that purpose we use a concept called exponential stability.

Definition A.4 ([36]) *An equilibrium point **0** is exponentially stable if there exist two strictly positive numbers α and λ such that*

$$\forall t > 0, ||x(t)|| \leq \alpha ||x(0)|| e^{-\lambda t} \tag{A.2}$$

in some ball S_r around the origin, with λ being the rate of exponential convergence.

We say that a system is exponentially stable if the state vector of the system converges to the origin faster than an exponential function. Exponential stability implies asymptotic stability, but asymptotic stability does not guarantee exponential stability.

All of the above definitions refer to the local behaviour of the system, however, if we want to know how the system behaves for any initial state, we have to redefine the concepts above.

Definition A.5 ([36]) *If asymptotic (or exponential) stability holds for any initial states, the equilibrium point is said to be globally asymptotically (or exponentially) stable.*
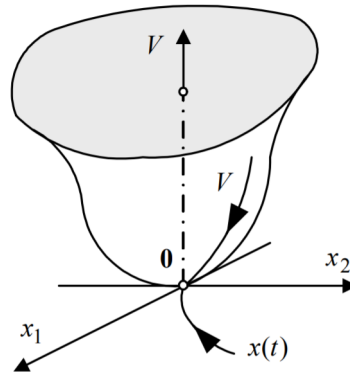
Figure A.2: Illustrating definition A.7 for n=2 [36]

A.2   Lyapunov Functions

Before we introduce Lyapunov functions, there is an important concept that should be formalized, which is the concept of positive-definite functions.

Definition A.6 ([36]) *A scalar continuous function $V(x)$ is said to be* <u>*locally positive definite*</u> *if* $V(0) = 0$ *and, in a ball S_{R_0}*

$$x \neq 0 \Rightarrow V(x) > 0 \tag{A.3}$$

If $V(0) = 0$ and the above property holds over the whole state space, then V(x) is said to be <u>*globally positive definite*</u>*.*

The above definition implies that the function V has a unique minimum at the origin 0. If $V(x)$ actually contains the origin 0,

$$V(0) = 0 \wedge x \neq 0 \Rightarrow V(x) \geq 0, \tag{A.4}$$

then the function is called *positive semi-definite*.

Similarly, the same concepts can be defined for negative or semi-negative definite functions.

Knowing this, we can now define a special type of functions, usually called Lyapunov functions.

Definition A.7 ([36]) *If, in a ball S_{R_0}, the function $V(x)$ is positive definite and has continuous partial derivatives, and if its time derivative along any state trajectory is negative semi-definite, i.e.,*

$$\dot{V}(x) \leq 0 \tag{A.5}$$

then $V(x)$ is said to be a <u>*Lyapunov function*</u>*.*

A.3   Equilibrium Point and Invariant Set Theorems

With the concepts presented above, we can now make a relation between Lyapunov functions and stability.

Theorem A.1 *Local Stability ([36]) If, in a ball S_{R_0}, there exists a scalar function $V(x)$ with continuous first partial derivatives such that*

- *$V(x)$ is positive definite (locally in S_{R_0})*

- *$\dot{V}(x)$ is negative semi-definite (locally in S_{R_0})*

then the equilibrium point 0 is stable. If, actually, the derivative $\dot{V}(x)$ is locally negative definite in S_{R_0}, then the stability is asymptotic. S_{R_0} is the domain of attraction.

For global stability, an additional condition has to be considered, because the ball S_{R_0} has to cover the whole state-space.

Theorem A.2 *Global Stability ([36]) Assume that there exists a scalar function V of the state x, with continuous first order derivatives such that*

- *$V(x)$ is positive definite*

- *$\dot{V}(x)$ is negative definite*

- *$V(x) \to \infty$ as $||x|| \to \infty$*

then the equilibrium at the origin is globally asymptotically stable.

Sometimes, however, not every condition is met to guarantee the system stability, particularly when $\dot{V}$, the derivative of the Lyapunov function candidate, is only semi-definite negative. When this happens, to conclude if the system is asymptotically stable, we have to address the invariant set theorems. Let us first introduce the definition of invariant set.

Definition A.8 ([36]) *A set G is an invariant set for a dynamic system if every system trajectory which starts from a point in G remains in G for all future time.*

Now we can present the invariant set theorem.

Theorem A.3 *(Local Invariant Set Theorem) ([36]) Consider an autonomous system of the form $\dot{x} = f(x)$, with f continuous, and let $V(x)$ be a scalar function with continuous first partial derivatives. Assume that*

- *for some $l > 0$, the region Ω_l defined by $V(x) < l$ is bounded*

- *$\dot{V}(x) \leq 0$ for all x in Ω_l*

Let R be the set of all points within Ω_l where $\dot{V}(x) = 0$, and M the largest invariant set in R. Then, every solution $x(t)$ originating in Ω_l tends to M as $t \to \infty$.

Appendix B

Detailed Simulink Model

The 3D Simulink Model used in our simulations is detailed in this appendix.
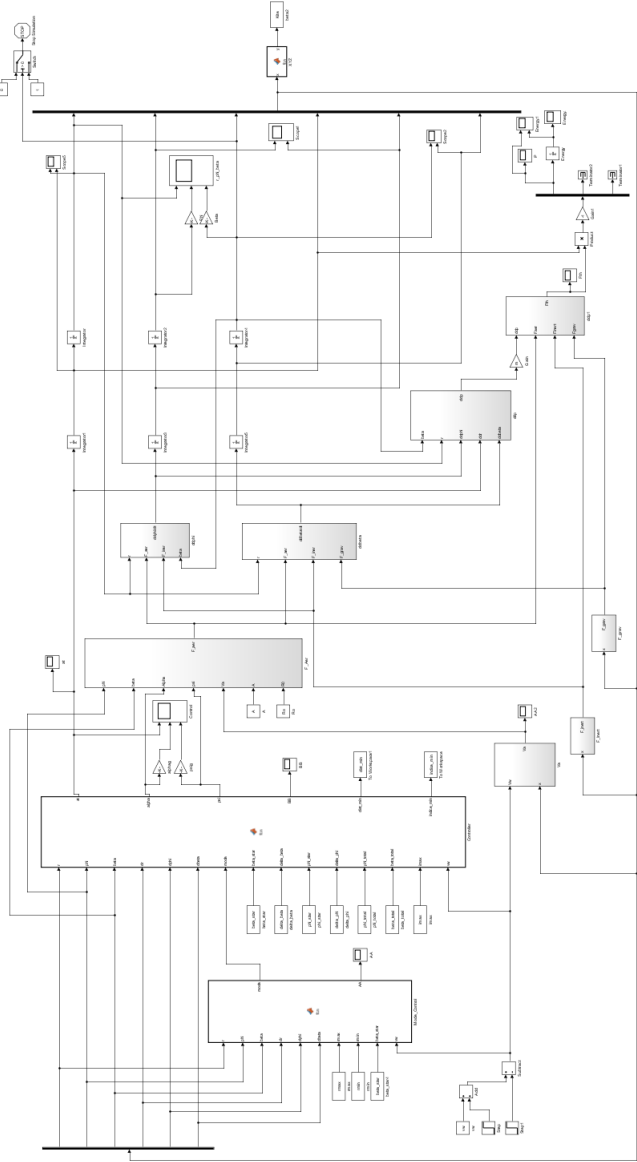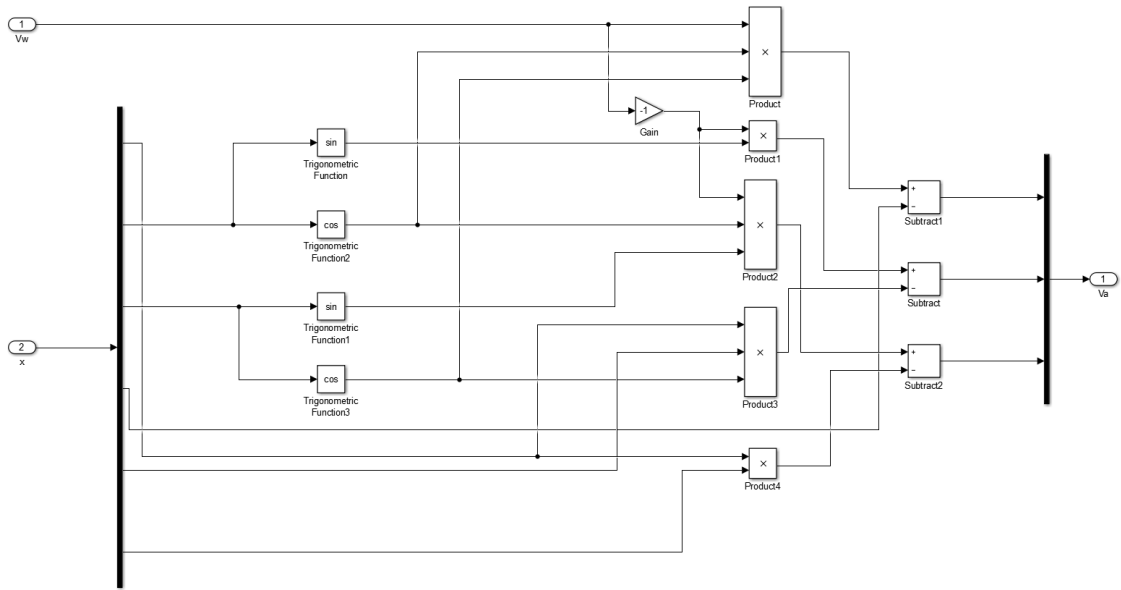
Figure B.1: Complete Simulink 3D Model
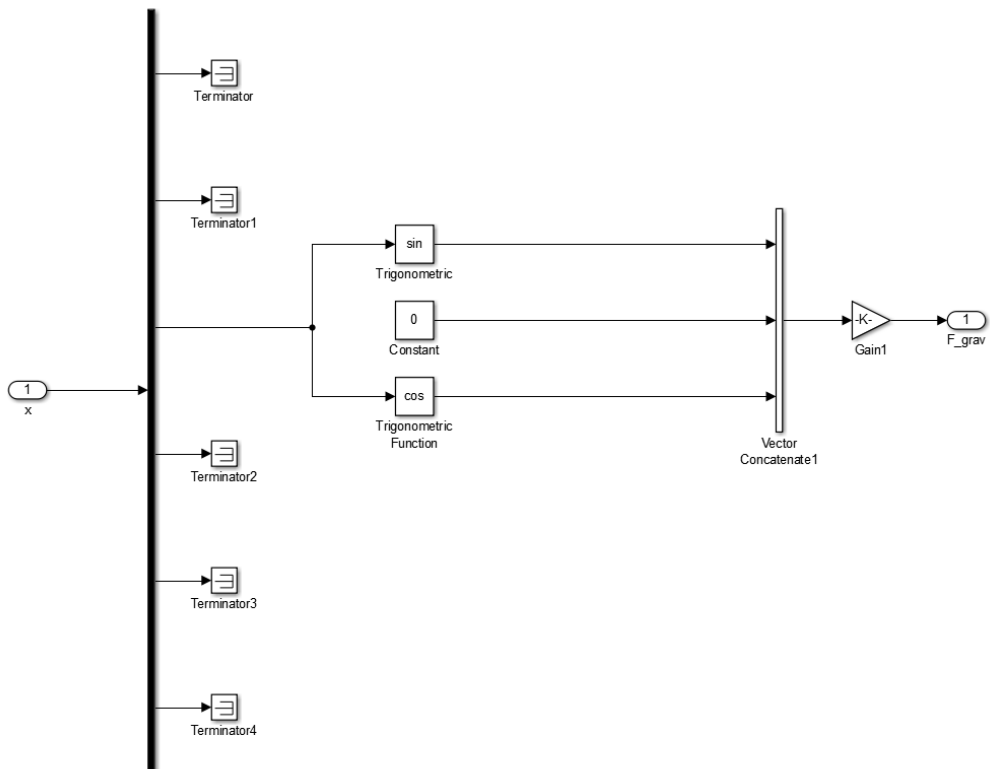
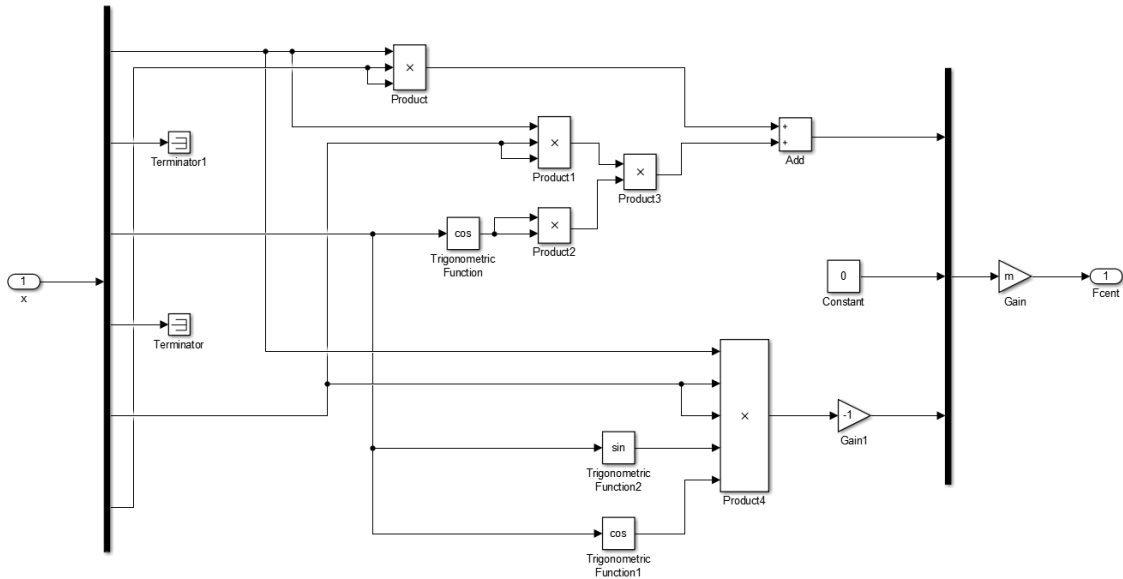Figure B.2: Va Subsystem

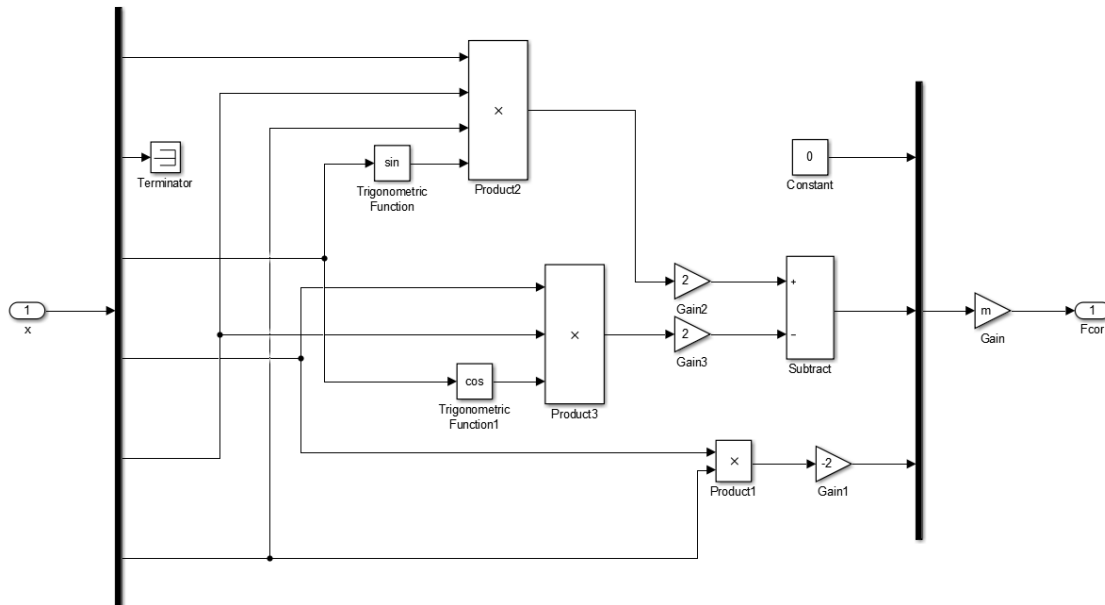Figure B.3: Gravity Force Subsystem

Figure B.4: Centripetal Force Subsystem
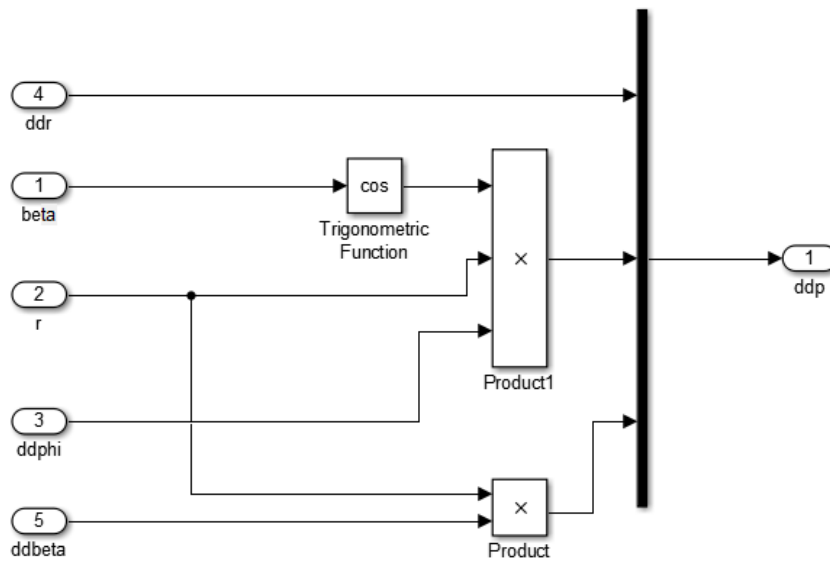

Figure B.5: Coriolis Force Subsystem
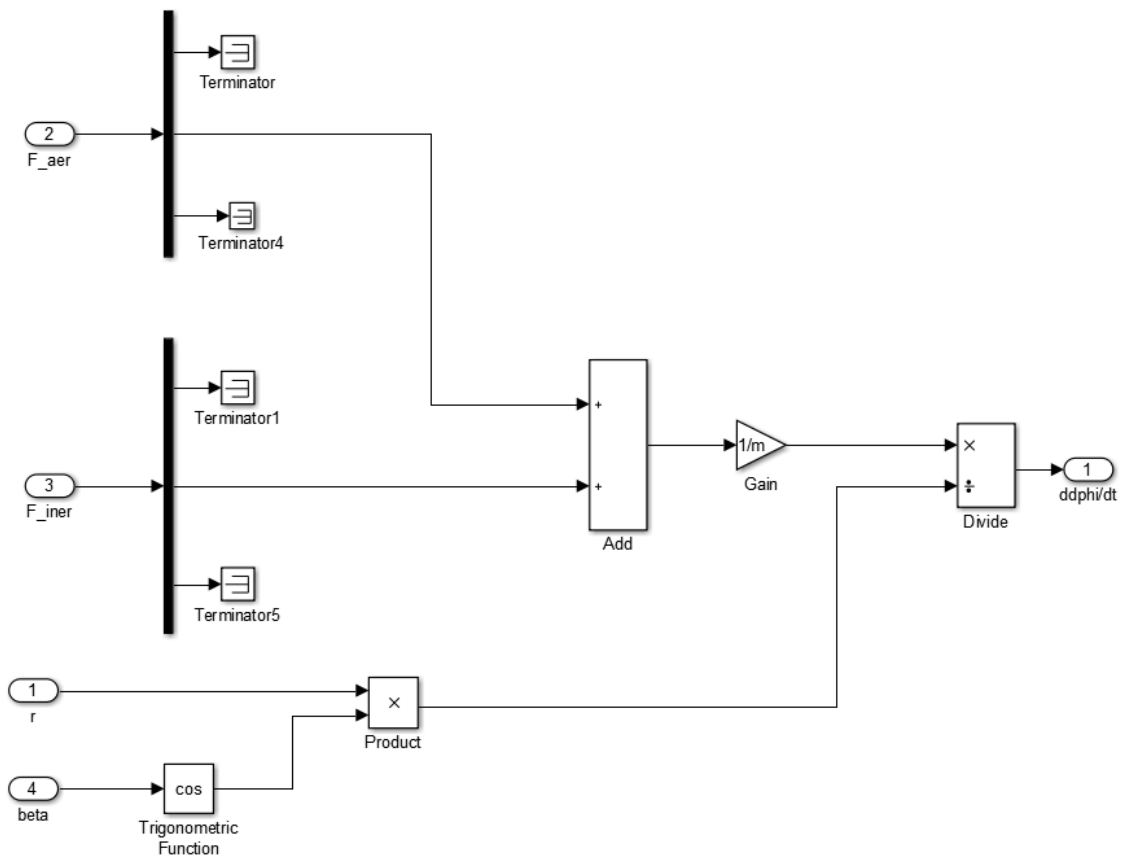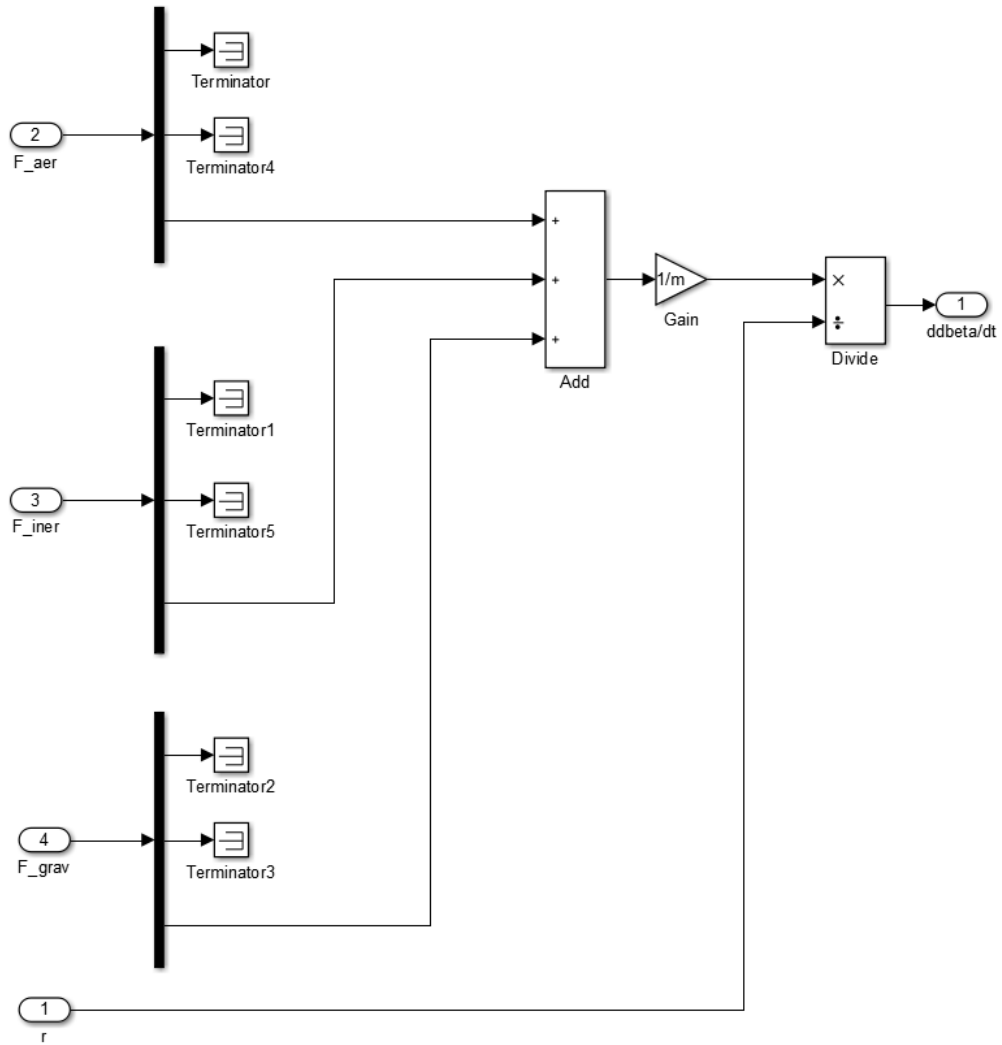
Figure B.6: $\ddot{p}$ Subsystem

Figure B.7: $\ddot{\phi}$ Subsystem

Figure B.8: $\ddot{\beta}$ Subsystem

References

[1] Miles L. Loyd. Crosswind kite power. *Journal of Energy*, 4(3):106–111, 1980. `doi:10.2514/3.48021`.

[2] Manuel C.R.M. Fernandes, Gonçalo B. Silva, Luís Tiago Paiva, and Fernando A.C.C. Fontes. A Trajectory Controller for Kite Power Systems with Wind Gust Handling Capabilities. In *Proceedings of 15th International Conference on Informatics in Control, Automation and Robotics (ICINCO)*, Porto, 2018 - to appear.

[3] Renewables fully meet Portugal's power needs in March, April 2018. URL: `https://windeurope.org/newsroom/news/renewables-fully-meet-portugals-power-needs-in-march/`.

[4] Kronsbein. Wind Power Capacity Worldwide reaches 539 GW, February 2018. URL: `http://www.sunwindenergy.com/wind-energy/wind-power-capacity-worldwide-reaches-539-gw`.

[5] Uwe Ahrens, Moritz Diehl, and Roland Schmehl, editors. *Airborne Wind Energy*. Green Energy and Technology. Springer Berlin Heidelberg, Berlin, Heidelberg, 2013.

[6] Roland Schmehl. *Airborne Wind Energy: Advances in Technology Development and Research*. Springer, 2018.

[7] Fernando A.C.C. Fontes and Luís Tiago Paiva. UP WIND Project, 2017. URL: `http://www.upwind.pt`.

[8] Sanghyuk Park, John Deyst, and Jonathan How. A New Nonlinear Guidance Logic for Trajectory Tracking. In *AIAA Guidance, Navigation, and Control Conference and Exhibit*. American Institute of Aeronautics and Astronautics. URL: `https://arc.aiaa.org/doi/abs/10.2514/6.2004-4900`, `doi:DOI:10.2514/6.2004-4900`.

[9] Antonello Cherubini. *Advances in Airborne Wind Energy and Wind Drones*. PhD, Scuola Superiore Sant'Anna, Pisa, Italy, 2017.

[10] Antonello Cherubini, Andrea Papini, Rocco Vertechy, and Marco Fontana. Airborne Wind Energy Systems: A review of the technologies. *Renewable and Sustainable Energy Reviews*, 51(Supplement C):1461–1476, November 2015. URL: `http://www.sciencedirect.com/science/article/pii/S1364032115007005`, `doi:10.1016/j.rser.2015.07.053`.

[11] Mario Zanon, Sébastien Gros, Joel Andersson, and Moritz Diehl. Airborne wind energy based on dual airfoils. *IEEE Transactions on Control Systems Technology*, 21(4):1215–1222, 2013.

[12] Wubbo J. Ockels. Laddermill, a novel concept to exploit the energy in the airspace. *Aircraft Design*, 4:81–97, June 2001. doi:10.1016/S1369-8869(01)00002-7.

[13] KitePower. Kite Power, 2017. URL: https://www.tudelft.nl/en/ae/organisation/departments/aerodynamics-wind-energy-flight-performance-and-propulsion/wind-energy/research/kite-power/.

[14] Paul Williams, Bas Lansdorp, and Wuboo Ockels. Modeling and control of a kite on a variable length flexible inelastic tether. In *AIAA Modeling and Simulation Technologies Conference and Exhibit*, page 6705, 2007.

[15] Kitepower B.V. Kitepower - Airborne Wind Energy. URL: https://kitepower.nl/.

[16] KiteGen. URL: http://kitegen.com/.

[17] EnerKíte. EnerKíte - Airborne Windenergy Converters, 2017. URL: http://www.enerkite.de/en/.

[18] Tiago Maia. Optimal Control of Power Kites for Wind Power Production. Master's thesis, Universidade do Porto, 2013.

[19] Massimo Canale, Lorenzo Fagiano, and Mario Milanese. Power kites for wind energy generation. *IEEE Control Systems Magazine*, 27(6):25–38, 2007.

[20] AmpyxPower. Ampyx Power, 2017. URL: https://www.ampyxpower.com/.

[21] TwingTec. Twingtec – Wind Energy 2.0, 2017. URL: http://twingtec.ch/.

[22] Omnidea | aerial platforms. URL: https://www.omnidea.net/aerial-platforms.

[23] MakaniPower. Makani | Makani, 2017. URL: https://x.company/makani/.

[24] Altaeros. URL: http://www.altaeros.com/.

[25] Magenn Power Inc. URL: https://www.sdtc.ca/en/organizations/magenn-power-inc.

[26] Airborne Wind Energy becomes Mainstream with Shell, E.ON Investment. URL: https://daidalos-capital.com/airborne-wind-energy-becomes-mainstream-with-shell-e-on-investment/.

[27] Ampyx Power collaborates with E.ON to commercialize Airborne Wind Energy, April 2017. URL: https://www.ampyxpower.com/2017/04/ampyx-power-collaborates-with-e-on-to-commercialize-airborne-wind-energy.

[28] Luís Tiago Paiva and Fernando A. C. C. Fontes. Optimal Control Algorithms with Adaptive Time-Mesh Refinement for Kite Power Systems. *Energies*, 11(3):475, February 2018. URL: http://www.mdpi.com/1996-1073/11/3/475, doi:10.3390/en11030475.

[29] M. Canale, L. Fagiano, and M. Milanese. High Altitude Wind Energy Generation Using Controlled Power Kites. *IEEE Transactions on Control Systems Technology*, 18(2):279 – 293, 2010.

[30] Aero: Angle of Attack. URL: http://code7700.com/aero_angle_of_attack.htm.

[31] Luis Tiago Paiva and Fernando ACC Fontes. Optimal control of underwater kite power systems. In *Energy and Sustainability in Small Developing Economies (ES2DE), 2017 International Conference in*, pages 1–6. IEEE, 2017.

[32] The Lift Equation. URL: https://www.grc.nasa.gov/www/k-12/airplane/lifteq.html.

[33] CLARK Y AIRFOIL (clarky-il). URL: http://airfoiltools.com/airfoil/details?airfoil=clarky-il.

[34] L. Fagiano, A. U. Zgraggen, M. Morari, and M. Khammash. Automatic Crosswind Flight of Tethered Wings for Airborne Wind Energy: Modeling, Control Design, and Experimental Results. *IEEE Transactions on Control Systems Technology*, 22(4):1433–1447, July 2014. doi:10.1109/TCST.2013.2279592.

[35] Philip Bechtle, Thomas Gehrmann, Christoph Sieg, and Udo Zillmann. AWEsome: An open-source test platform for airborne wind energy systems. *arXiv preprint arXiv:1704.08695*, 2017.

[36] Jean-Jacques E Slotine, Weiping Li, and others. *Applied nonlinear control*, volume 199. Prentice hall Englewood Cliffs, NJ, 1991.